Arab Hassani. *Soft Sci* 2023;3:31
DOI: 10.20517/ss.2023.23

Soft Science

Review Article

Open Access

Bioreceptor-inspired soft sensor arrays: recent progress towards advancing digital healthcare

Faezeh Arab Hassani*

School of Electrical, Electronic, and Mechanical Engineering, University of Bristol, Bristol BS8 1UB, United Kingdom.

***Correspondence to:** Dr. Faezeh Arab Hassani, School of Electrical, Electronic, and Mechanical Engineering, University of Bristol, 75 Woodland Road, Bristol BS8 1UB, United Kingdom. E-mail: faezeh.arabhassani@bristol.ac.uk

How to cite this article: Arab Hassani F. Bioreceptor-inspired soft sensor arrays: recent progress towards advancing digital healthcare. *Soft Sci* 2023;3:31. https://dx.doi.org/10.20517/ss.2023.23

Received: 15 May 2023 **First Decision:** 14 Jun 2023 **Revised:** 3 Aug 2023 **Accepted:** 11 Aug 2023 **Published:** 24 Aug 2023

Academic Editor: Zhifeng Ren **Copy Editor:** Pei-Yun Wang **Production Editor:** Pei-Yun Wang

Abstract

Recent advances in soft sensor technology have pushed digital healthcare toward life-changing solutions. Data reliability and robustness can be realised by building sensor arrays that collect comprehensive biological parameter data from several points on the underlying organs simultaneously, a principle that is inspired by bioreceptors. The rapid growth of soft lithography and printing, three-dimensional (3D) printing, and weaving/knitting technologies has facilitated the low-cost development of soft sensors in the array format. Advances in data acquisition, processing, and visualisation techniques have helped with the collection of meaningful data using arrays and their presentation to users on personal devices through wireless communication interfaces. Local- or cloud-based data storage helps with the collection of adequate data from sensor arrays over time to facilitate reliable prognoses based on historical data. Emerging energy harvesting technologies have led to the development of techniques to power sensor arrays sustainably. This review presents developmental building blocks in wearable and artificial organ-based soft sensor arrays, including bioreceptor-inspired sensing mechanisms, fabrication methods, digital data-acquisition techniques, methods to present the results to users, power systems, and target diseases/conditions for treatment or monitoring. Finally, we summarise the challenges associated with the development of single and multimodal array sensors for advanced digital healthcare and suggest possible solutions to overcome them.

Keywords: Bioreceptor-inspired, soft sensor arrays, multimodal, senses of vision, hearing, taste, smell, spatial perception

INTRODUCTION

Low energy requirements and high sensitivity are two of the characteristics of biological receptors[1]. The

responses of biological receptors (i.e., mechano, thermoreceptors, photo, chemo, electro, and magneto) to internal or external stimuli constitute the foundation of remarkable innovations in wearable sensing technology[2]. Receptor organs, such as the eyes, ears, nose, mouth, and internal organs, contain various types of receptor cells that promote parallel sampling and processing of sensory information[3].

Receptor types include neurons with free nerve endings embedded in tissues, neurons with encapsulated endings in connective tissues, or specialised receptor cells with specific structures and sensitivity to specific types of stimuli[4]. Two examples of neurons with free endings are pain and temperature receptors in the skin dermis (i.e., mechano and thermoreceptors, respectively)[5]. Mechanoreceptors are divided into three groups: Tactile receptors, proprioceptors, and baroreceptors[6-8]. Tactile mechanoreceptors in the skin include Merkel's disks with free nerve endings, Meissner's corpuscles, Ruffini endings, and Pacinian corpuscles with encapsulated endings located near the skin surface, as well as deeper-level Krause end bulb receptors with encapsulated endings in specialised regions[6]. Proprioceptors can be found in the skin, joint capsules, tendons, muscles, ligaments, and connective tissue, and they contribute to the position and movement senses[8]. Baroreceptors in the walls of blood vessels allow for the transfer of blood pressure information to the autonomic nervous system[7]. Thermoreceptors detect and respond to changes in temperature. They can be found on the skin and inside the body[9]. Specialised receptor cells called photoreceptors in the retina respond to light stimuli[10]. The nasal cavity houses olfactory receptor neurons as chemoreceptors that respond to smells. The biomechanical activity of prey animals generates electric fields that can be detected by electroreceptor cells on the skin of animals[11]. Magnetoreceptor cells in animals' skin allow them to detect geomagnetic fields for different purposes related to navigation[12].

On the basis of the operating principles of bioreceptors, arrays of various types of sensors have been developed and used to mimic receptor organs[13-17]. Figure 1 presents schematics of the photo, electro, mechano, olfactory, taste, and auditory bioreceptors, which are responsible for the vision, touch, spatial perception, smell, taste, and hearing senses, respectively[18-23]. Table 1 summarises the specific functions and limitations of these six bioreceptors and the health conditions that could affect their performance[24-46]. In addition, it lists suitable characteristics of the biomimetic soft sensor arrays that could replace these bioreceptors, namely high sensitivity, resolution, selectivity, short response time, and high stability. In what follows, we provide examples of soft sensors, explain their fundamental concepts, discuss the associated materials, and summarise the functionalities needed to replicate the performance of these bioreceptors.

Nanowire-based photodetectors and phototransistors are examples of sensors that can respond to light similarly to photoreceptors[47]. Semiconductors (e.g., III-V semiconductors, metal oxides, perovskites, *etc.*) are the most common materials used to fabricate nanowire-based photodetectors. Photoconductivity is a known phenomenon in semiconductors, where incident light could lead to an increase in electrical conductivity through the photogeneration of carriers[47]. These nanowire-based photodetectors could be fabricated as single nanowires or an ensemble (forest) of vertical nanowire arrays[48]. Vertical nanowire array photodetectors grown on flexible polymer substrates performed well in terms of restoring light responses when replacing degenerated photoreceptors in the retina[49]. Meanwhile, the light incident on a phototransistor can modulate the channel charge carrier density by acting as an additional optically controlled terminal apart from the three conventional transistor terminals. Metal oxide semiconductor field-effect transistor (MOSFET)-type photodetectors (i.e., phototransistors) fabricated on flexible polymer substrates offer high photosensitivity and responsivity, thereby mimicking the behaviour of mammalian eyes[50]. To detect colours similarly to cone cells in the eye, Zheng *et al.* used three types of nanoparticle solutions, namely gold nanorods (Au NR), gold nanospheres (Au NS), and silver NS (Ag NS), to fill the holes of a flexible polydimethylsiloxane (PDMS) substrate[51]. One hole was filled with a carbon nanoparticle

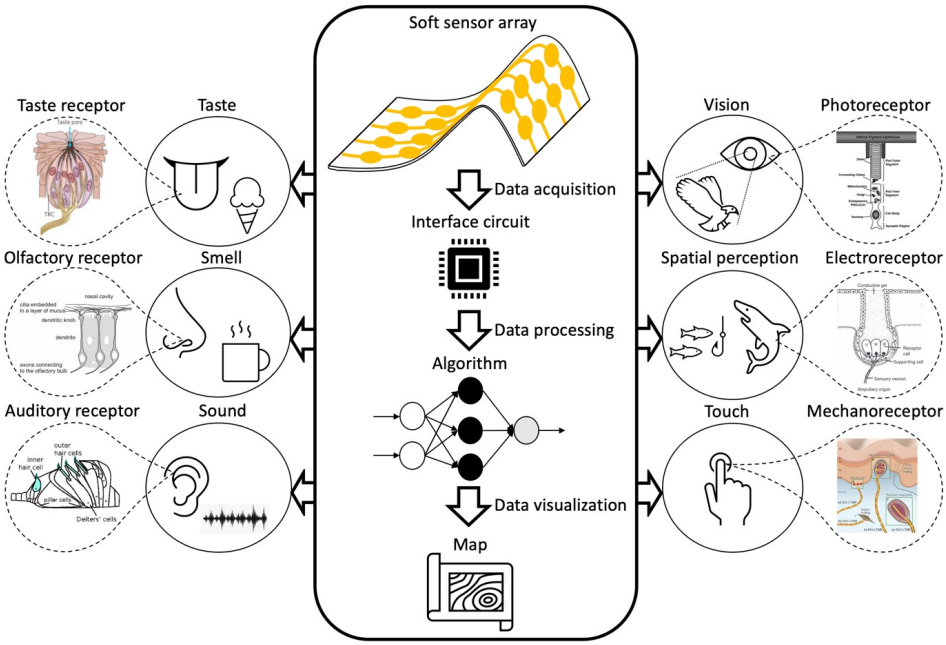

Figure 1. Schematic illustration of various receptors responsible for vision, perception, touch, taste, smell, and hearing, and potential of soft sensor arrays to mimic their operation with the help of additional interface circuits, data processing, and visualisation techniques. Figure "photoreceptor", quoted with permission from Murray *et al.*[18]; "electroreceptor", quoted with permission from Kibenge *et al.*[19]; "mechanoreceptor", reprinted with permission from AAAS[20]; taste receptor, quoted with permission from Chandrashekar *et al.*[21]; "olfactory receptor"[22], and "auditory receptor"[23].

Table 1. Characteristics and limitations of six bioreceptors

Receptor type	Main function	Limitation	Health conditions affecting their performance	Ideal sensor array performance
Photoreceptor[24-28]	Respond to light intensity, colour, and motion	Sensitive to damage from prolonged intense visible light exposure	Ageing, retinal diseases, and macular degeneration	A wide field of view (FOV) of 150°-160°, high resolution of 1 arcmin per line pair at the fovea, and adaptivity to various optical environments
Electroreceptor[29-31]	Respond to electrical potential differences	Disturbed by anthropogenic electric fields	Environmental effects and damage to the sensory system	Respond to electric fields ranging from a few microvolts per centimetre to 100 $\mu V \cdot cm^{-1}$
Mechanoreceptor[32-35]	Respond to vibration, touch, pressure, and sound	Oversensitivity causes painful sensations upon light touch (i.e., Allodynia)	Ageing and dysregulation of neuromuscular signalling	Respond to load changes in a frequency range of 0.3-500 Hz, with a response time of 40 ms or lower and high sensitivity in a broad pressure detection range of 0 to a few hundred kPa
Taste receptor[36-39]	Respond to taste substances	Decreased sensitivity in response to chronic exposure to a specific tastant	Ageing, chemosensory disorders, and neurological diseases	Respond to sweet, salty, sour, bitter, umami, and fat tastes within a few tens of milliseconds
Olfactory receptor[40-42]	Respond to odours	Decreased sensitivity in response to constant or repetitive exposure to an odour	Ageing and neurodegenerative disorders	Respond to various odours with detection thresholds ranging from 10^{-6} to 10^{3} ppm
Auditory receptor[43-46]	Respond to sound	Upper frequency limit of 15 kHz for hearing in young adults and loss of hearing sensitivity and auditory acuity resulting from exposure to excessive sound levels	Ageing, exposure to ototoxic compounds, including drugs, and infections	Respond to 1.5 Hz-15 kHz sounds with normal hearing at sound pressure levels of 0-120 dB (discomfort threshold)

(C NP) solution to achieve a brightness response similar to that of rod cells. Indium tin oxide (ITO) layers were patterned on the top and bottom of each solution-filled hole to detect changes in electrical signals in response to incident light.

Electrostatic induction sensors can mimic the operation of electroreceptors. Sometimes, these sensors include an electrode layer embedded in an insulating layer. If any naturally charged object approaches the electrode, changes in electrical output are detected through electrostatic induction. If the electrode is exposed to the object, both charge transfer due to physical contact and electrostatic induction occur[52]. Another example is a sensor consisting of a top layer composed of a pre-charged elastomeric electret, a layer of conductive hydrogel acting as the ionic electrode, and a flexible insulating substrate. When a naturally charged object approaches the top electret layer, the charge transfer induced in the ionic electrode generates an electrical output[53].

Flexible capacitive, resistive, piezoelectric, and triboelectric pressure sensors can be used to detect low- and medium-pressure stimuli, similar to the mechanoreceptors in the skin[54-56]. Resistive pressure sensors comprise a soft/flexible pressure-sensitive conductive layer [e.g., carbon nanotubes (CNTs) and PDMS composite materials], the resistivity of which changes with the application of a pressure stimulus. Capacitive sensors consist of a soft insulating layer (e.g., PDMS) sandwiched between two electrodes, and the capacitance value of the sensor changes when it is subjected to pressure. The piezoelectric effect observed in materials such as poly(vinylidene fluoride) (PVDF) is used to convert applied pressure into voltage changes in piezoelectric sensors[57]. In triboelectric sensors, alternating contact and separation of two materials with different electron affinities [e.g., polytetrafluoroethylene (PTFE) and aluminium (Al) layers[58]] during pressure application induces surface charge generation (i.e., triboelectric effects)[59,60].

Various types of sensors, such as biosensors, electrochemical, surface acoustic wave (SAW), resistive, colourimetric, and optical sensors, have been developed to mimic olfactory receptors[61]. For example, a chemoreceptive ion gel was patterned on top of the poly(3,4-ethylenedioxythiophene) polystyrene sulfonate (PEDPT:PSS) channel of an organic electrochemical transistor (OECT) to realise an electrochemical olfactory sensor on a flexible substrate. The interaction of gas molecules with the ions in the ion gel generates a potential that, in turn, gates the OECT channel[62].

Various types of chemical sensors[63] and enzyme-modified triboelectric sensors[64] have been developed to mimic taste receptors. Chemical sensors are potentiometric or amperometric devices with sensing layers (e.g., ion-selective and artificial lipid polymer membranes, metal oxides, and bioreceptors such as enzymes, antibodies, nucleic acids, and cells[65]) that can detect a wide range of taste substances by measuring electrical potential or current[66]. One example of a flexible chemical sensor consists of laser-induced graphene interdigitated electrodes (IDEs) patterned on a polyimide (PI) film and transferred onto a flexible Kapton tape[67].

Acoustic sensors based on piezoelectric, triboelectric, capacitive, or piezoresistive mechanisms can mimic auditory receptors[68,69], and their operating principles are the same as those of mechanoreceptors. However, the stimulus for acoustic sensors is sound. For example, a piezoelectric acoustic sensor on a thin flexible polyethylene terephthalate (PET) substrate comprises a lead-zirconate-titanate (PZT) membrane with multichannel IDEs for realising multi-resonant frequency band control that covers the entire voice spectrum, similar to the human ear[70].

The significance of the use of these flexible sensors in bioreceptor-inspired sensor arrays lies in their potential to offer large-area sensing, unprecedented sensitivity, selectivity, conformability, and energy efficiency by mimicking the mechanisms used in natural biological systems[71-74]. This can greatly enhance the fields of health monitoring, disease detection, environmental monitoring, and so on[75,76].

Soft bioinspired sensor arrays that are compatible with complex biological organs could help mimic natural senses with the help of data acquisition [i.e., signal conditioning and analogue-to-digital conversion (ADC) circuits], data processing, and visualisation techniques[77], as presented in Figure 1. Signal conditioning involves signal amplification and noise filtering. Sensor signals are typically amplified by transistors. By using transistor-based sensor arrays, such as OECT arrays, the intrinsic gain of transistors can be used to obtain amplified signals at low applied voltages[78,79]. Chemical sensor arrays can help discriminate various similar analytes, recognise specific patterns, and ease data processing for complex samples[80]. Pressure sensor arrays can track spatial pressure and map pressure changes with high resolution[81]. These arrays have been developed in various formats, such as second skin/patches, lenses, artificial organs, and clothes[82-84].

The aforementioned sensor array systems are often integrated with actuating/electrical stimulation elements to realise closed-loop systems; such systems are useful for developing smart systems that operate similarly to biological organs in the body[59,85-88]. Biochemical [e.g., glucose and pH, thermal (temperature), mechanical (e.g., strain and pressure)], and electrical [e.g., electroencephalogram (EEG) and electrocardiogram (ECG)] signals detected using body sensors can change because of diseases. To regulate these changes, biochemical, mechanical, and electrical actuators can be used for biochemical production, organ stimulation, and neural stimulation, respectively[89,90]. For example, the pancreas is responsible for lowering blood sugar levels by releasing insulin[91]. In patients with type 1 diabetes, this regulation needs to be maintained using insulin pumps[92]. If a sensor can detect the blood sugar level, and based on this reason, if an actuator can release an adequate amount of insulin, a closed-loop system can be formed (i.e., artificial pancreas). These actuators are usually inspired by nature[93-98]. For instance, the octopus vulgaris arm with several suckers and an interconnected nervous system has inspired the development of a soft adhesion actuator that consists of a sucker with integrated strain sensors capable of picking up objects[99]. Then, strain sensors can be used to measure the mass of such objects and activate the actuator to ensure that it is firmly attached to the object.

The use of bioinspired and biomimetic strategies to develop energy storage and harvesting devices could enhance and optimise the performances of these closed-loop systems[100-106]. The electricity generated by bioinspired energy harvesting devices, such as triboelectric[107] and piezoelectric nanogenerators[108] and solar cells[109], can be stored in storage units and used to power electronic devices[110]. The two examples that are inspired by nature are electrode design and materials of lithium-ion batteries and the solid-solid electrode/electrolyte interfaces in solid-state batteries[100].

SOFT SENSOR ARRAYS TO REBUILD KEY SENSES

Several reviews have focused on bioinspired electronics. Valle[111] and Jung *et al.*[112] reviewed bioinspired sensing systems based on the five traditional senses, namely the vision, touch, taste, smell, and auditory senses. Xiao *et al.*[113] focused on bioinspired ionic sensory systems, while Li *et al.*[114] explored the prosthetic interface applications of bionic sensor systems. Xue *et al.* summarised the processes and applications of bioinspired sensor systems in healthcare[115]. However, the present review focuses on bioreceptor-inspired sensors and actuator arrays fabricated on a single soft, flexible substrate to rebuild one of the senses, such as vision, spatial perception, touch, taste, smell, and hearing, to treat/monitor a specific condition or in prosthetic applications. A summary of the key characteristics of the explored soft sensor and actuator/electrode arrays is presented in Table 2 and discussed in the subsequent text[27,116-129]. This review focuses on the bioreceptors that have inspired the development of sensor arrays, circuits required to build data acquisition and processing units, power sources used in various systems, array fabrication processes, and target healthcare applications.

Table 2. Summary of key characteristics of soft sensor arrays used to treat/monitor a specific condition or prosthetic application

Bioreceptor-inspiration type (Sense)	Sensor/Actuator type (Application format)	Single or multimodal sensing (Detected stimuli)	Data acquisition, data processing, and data visualisation	Soft/Flexible substrate	Powering system	Target healthcare application
Photoreceptor (Vision)[27]	Nanowire array as photosensor (Artificial eye)	Single (Light)	Multiplexer, pre-amplifier, and current meter; personal computer; and image reconstruction and visualisation	Porous aluminium oxide membrane /PDMS	Power supply	Humanoid robots
Photoreceptor (Vision)[116]	Phototransistor and electrode array (Artificial retina)	Single (Light and electrical stimulation)	Soft flexible printed circuit board that includes trans-amplifier, inverter, and micro-controller unit (MCU); image processing electronics; and image visualisation	PI	Cell battery and power supply	Retinal prosthesis
Electroreceptor (Spatial perception)[117]	Electrostatic induction receiver array (Patch)	Single (Object's electric field)	Electrometer; personal computer; and auditory signal generation	Hydrogel/Elastomer	Self-powered	Vision restoration
Mechanoreceptor (Virtual perception/touch)[118]	Vibration actuator array (Patch)	Single (Vibration)	Linear voltage regulator, near-field communication antennas, integrated circuit, personal computer, and sense of virtual touch	Silicone	Wirelessly powered	Virtual/Augmented reality
Mechanoreceptor (Touch)[119]	Capacitive pressure sensor array (Patch)	Single (Pressure)	LCR meter, personal computer, and pressure mapping	PDMS	Power supply	Health monitoring and interactive robotics
Mechanoreceptor (Touch)[120]	Capacitive pressure sensor array (Patch)	Single (Pressure)	LCR meter, neural network training, and quantum dot light-emitting diodes display and pressure mapping	PDMS	Power supply	Skin prosthetics
Mechanoreceptor (Touch)[121]	Resistive pressure sensor array (Patch)	Single (Pressure)	Signal converter, amplifier, noise-filtering, and ADC conversion; personal computer; and three-dimensional (3D) mapping	PDMS/PET	Power supply	Pulse monitoring
Mechanoreceptor (Touch)[122]	Triboelectric sensor array (Cloth)	Single (Pressure)	Amplifier, low-pass filter, ADC, and Bluetooth; mobile phone; and pressure signal	Textile	Self-powered	Cardiovascular disease and sleep apnoea syndrome assessments
Taste receptor (Taste)[123]	Electrode array (Patch)	Single (Chemical and electrical stimulation)	Portable low-voltage adjustable power supply stimulating module; personal computer; and radar map	PI	Battery	Non-invasive oral electrotherapy and brain-tongue-machine interface
Taste receptor (Taste)[124]	Ionic conductivity sensor array (Patch)	Single (Chemical)	Semiconductor characterisation system; personal computer; and map of current changes	PEN	Power supply	Taste-monitoring devices and humanoid robots
Olfactory receptor (Odour)[125]	Resistive sensor array (Armband)	Single (Chemical)	Voltage divider, analogue multiplexer, data acquisition device, and Zigbee; personal computer; PCA; and PCA plot	PEN	Power supply	Health monitoring
Olfactory receptor (Odour)[126]	Resistive sensor array (Armband)	Single (Chemical)	Voltage divider, MCU, and Bluetooth; personal computer and PCA; and PCA plot	PVDF/PET	Battery	Health monitoring and individual identification
Auditory receptor (Sound)[127]	Acoustic sensor array (Artificial ear)	Single (Sound)	Data acquisition card; sound source location algorithm and personal computer; and 3D mapping	PI	Self-powered	Sound identification and localisation
Mechanoreceptor (Touch)[128]	Triboelectric and pyroelectric sensor array (Patch)	Multi (Pressure and temperature)	Oscilloscope and source meter; personal computer; and 3D mapping	P(VDF-TrFE)	Self-powered	Health monitoring

Mechanoreceptor (Touch)[129]	Resistive, capacitive and photocurrent sensor array	Multi (Temperature, strain, humidity, and light magnetic fields)	LCR meter and parameter analyser; personal computer; and 3D mapping	PVA or PDMS	Power supply	Health monitoring, humanoid robotics, prosthetics, and human-machine interfaces

ADC: Analogue-to-digital conversion; MCU: micro-controller unit; PCA: principal component analysis; PDMS: polydimethylsiloxane; PEN: poly(ethylene naphthalate); PET: polyethylene terephthalate; PI: polyimide; PVA: poly(vinyl alcohol); PVDF: poly(vinylidene fluoride); P(VDF-TrFE): poly(vinylidene fluoride-trifluoroethylene).

Soft eye image-sensing arrays

The human eye comprises a lens that collects light and a hemispherical retina. Dense integration of 100-120 million photoreceptors and rod and cone cells in the retina helps convert incident light to action potentials that are transmitted to the brain through millions of nerve fibres [Figure 2A][27,130].

Gu *et al.* developed a biomimetic artificial electrochemical eye (EC-EYE) consisting of a hemispherical retina with a high-density perovskite nanowire array acting as the photosensor [Figure 2B][27]. An ionic liquid electrolyte mimicking vitreous humour served as the front-side common contact with the nanowires. Freestanding hemispherical porous aluminium oxide membranes (PAM) were used to grow a high-density array of perovskite nanowires inside nanochannels. Nanochannels were selectively opened in the PAM layer by using a focused ion beam. A magnetic field was used to align nickel (Ni) microneedles with three exposed nanowires on the PAM layer. Each Ni microneedle formed a pixel with a lateral size of 1 μm and pitch of 200 μm. Thin tubes filled with liquid metal were used to connect to each Ni microneedle through a PDMS socket. The PDMS socket was fabricated using a 3D-printed hedgehog-shaped mould to pattern a 10 × 10 hole array on the socket. Thin soft tubes filled with eutectic gallium indium liquid metal were used to form liquid-metal wires mimicking human nerve fibres behind the retina. Then, 100 such tubes were inserted into the PDMS socket holes, and the socket was attached to the PAM/nanowire surface to form the photodetector array. The liquid metal tubes were connected directly to a computer-controlled 100 × 1 multiplexer on a printed circuit board (PCB) [Figure 2C]. Several optical patterns (e.g., character "A") were projected onto the EC-EYE, and the photocurrent of each pixel was measured using a current meter. A personal computer (PC) was used for both processing the current data and controlling the multiplexer. The photocurrent values were converted to a grayscale number between zero and 255 to reconstruct the detected objects. Figure 2D shows the character "A" imaged by the EC-EYE and its projection onto a flat plane. The EC-EYE achieved a maximum photocurrent sensitivity of 303.2 mA/W, and the high-density nanowire arrays provided high image resolution. The EC-EYE was demonstrated as a vision system for humanoid robots that resembled the human eye in appearance and characteristics.

Unlike the EC-EYE, which reconstrued the entire eye, Choi *et al.* focused on developing a soft high-density image sensor and electrode array (i.e., a closed-loop system) integrated with the human retina, as shown in Figure 3A[116]. The device consists of a high-density, vertically stacked, and ultra-thin soft molybdenum disulfide (MoS_2)-graphene phototransistor (CurvIS) array and ultra-thin neural-interfacing electrodes (UNE) [Figure 3B]. Each stacked electrode and phototransistor is connected through a flexible PCB (FPCB) coated with soft and thick silicone rubber (i.e., soft FPCB). An external light signal is focused by the lens onto the CurvIS array [Figure 3B]. The output photocurrent generated by each phototransistor in response to the external light is amplified by a trans-impedance amplifier, passed through an inverter, and fed into a micro-controller unit (MCU). Figure 3C shows all these components integrated into the soft FPCB. The MCU measures and processes the amplified signal and generates electrical pulses. These electrical pulses are then applied to the relevant UNE

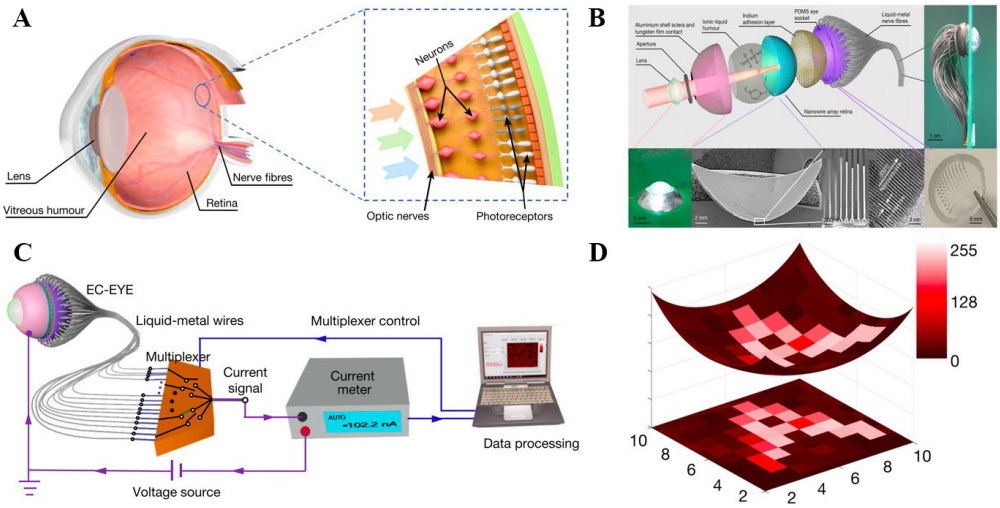

Figure 2. (A) Human eye and retina; (B) exploded, side, and top views of EC-EYE; low-resolution cross-sectional SEM image of hemispherical PAM/nanowires; cross-sectional SEM image of nanowires in PAM; high-resolution transmission electron microscopy image of a single-crystalline perovskite nanowire; and a photograph of the PDMS socket; (C) schematic illustration of measurement setup; and (D) image reconstructed (letter "A") by EC-EYE and its projection on a flat plane. This figure is quoted with permission from Gu *et al.*[27]. EC-EYE: Electrochemical eye; PAM: porous aluminium oxide membranes; PDMS: polydimethylsiloxane.

electrode to stimulate the retina [Figure 3D]. Moreover, the FPCB also includes image-processing electronics. Figure 3E shows optical camera images of the CurvIS array, UNE stack, and soft FPCB. To fabricate the UNE, chromium (Cr)/Au electrodes were patterned on a PI-coated silicon dioxide (SiO_2) wafer, followed by the deposition of a thin platinum (Pt) layer and a final PI encapsulation layer. A water-soluble tape was used to detach the UNE electrodes from the SiO_2 wafer and laminate them on the retina. The water-soluble tape was then dissolved. Similarly, the CurvIS phototransistor array included a stack of several layers on a thin PI film spin-coated onto a SiO_2 wafer. The layers included a thin layer of silicon nitride (Si_3N_4) as the transistor substrate, interdigitated graphene source/drain electrodes, an ultrathin photo-absorbing MoS_2 layer coated onto the graphene electrodes, an aluminium oxide (Al_2O_3) dielectric layer, a patterned titanium (Ti)/Au layer as the gate, and a final PI encapsulation layer. A water-soluble tape was used to detach the phototransistor array from the SiO_2 wafer. The tape was then shaped into a truncated icosahedron structure, stacked on the UNE, and laminated on the retina. The water-soluble tape was then dissolved. Figure 3F presents the university logo image captured by the CurvIS array. The phototransistor exhibited superior photoresponsivity than a silicon photodetector. This device could be used as an intraocular retinal prosthesis for patients with retinal degeneration, such as macular degeneration or retinitis pigmentosa.

Soft skin sensor arrays and virtual/augmented reality actuator arrays for perception

Some animals, such as sharks, skates, and rays, have electroreceptor network-embedded skins that allow them to locate nearby prey without making physical contact[131]. Each electroreceptor consists of two components: a soft ion-conducting hydrogel core that receives the electric fields generated by the prey animals and an ion-insulating epithelium that acts as a soft encapsulation layer for the hydrogel core [Figure 4A][53,132]. These animals compare the electric field intensity detected by each electroreceptor in the network to perceive the relative position of nearby prey (i.e., spatial perception)[132].

This sensing mechanism inspired Song *et al.* to develop a soft artificial electroreceptor (SAER), which is depicted in Figure 4B[117]. The SAER consists of a three-layer stack of 3D-printed conductive hydrogel on dielectric elastomers and an additional top-cover elastomer layer. The SAER attached to the hand of a subject is illustrated in Figure 4C. The middle layer is the sensing layer and consists of an array of four hydrogel electric field receivers. The bottom hydrogel layer that is in contact with the skin acts as a shield

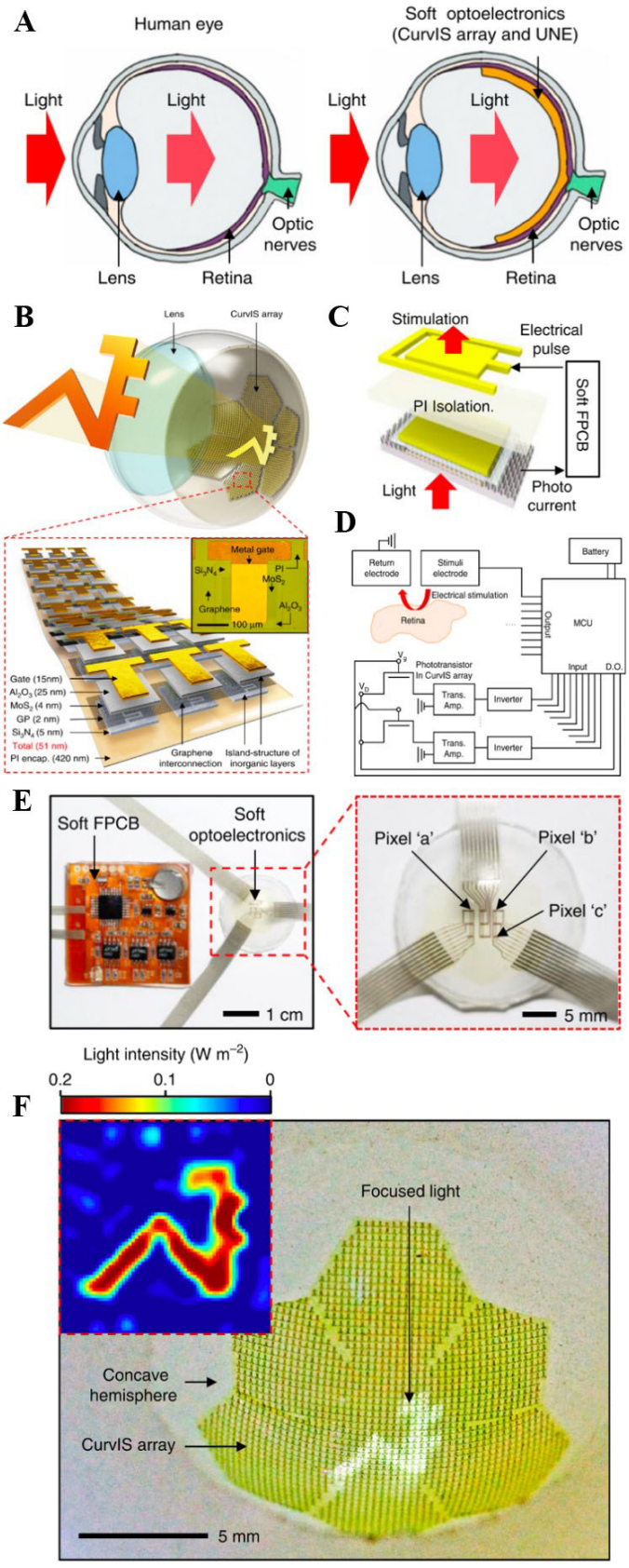

Figure 3. (A) Schematic illustration of the human ocular structure and the integrated soft optoelectronic device; (B) schematic illustration of the high-density CurvIS array based on the MoS_2-graphene heterostructure; (C) phototransistor stack (bottom) and the stimulation electrode (top) connected through the soft FPCB; (D) schematic illustration of the electronics for detecting external light

and stimulation; (E) optical camera image of the CurvIS array and UNE stack connected through the soft FPCB; and (F) university logo image captured by the CurvIS array[116]. FPCB: Flexible printed circuit board; UNE: ultra-thin neural-interfacing electrodes.

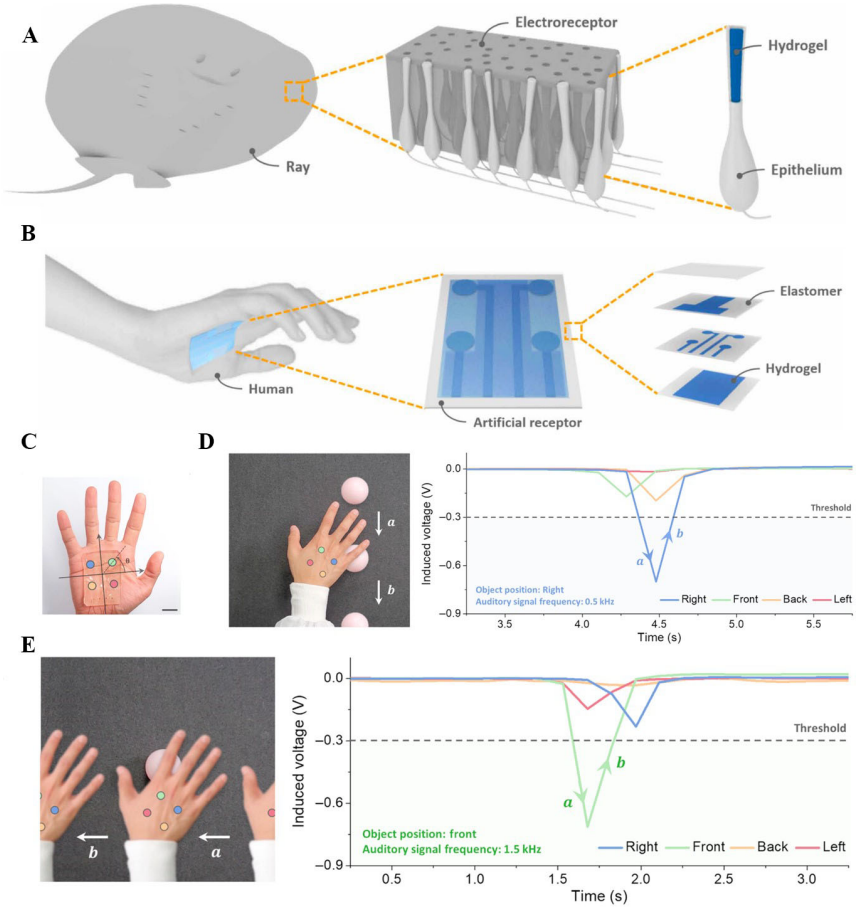

Figure 4. (A) Network of electroreceptors distributed on a ray's skin for locating nearby prey; (B) schematic illustration of wearable SAER on a hand; (C) image of wearable SAER attached to the hollow of the hand; (D) a person wearing the SAER to perceive spatial information of a dynamic object; and (E) a person wearing the SAER to perceive spatial information of a static object[117]. SAER: Soft artificial electroreceptor.

layer that blocks electrical noise from the skin of the subject. The top hydrogel layer acts as a shield layer, and it ensures that the voltage signal of the sensing layer electrodes is responsive to the distance of the external object, not its direction. To realise reliable adhesion of the 3D-printed hydrogel on the elastomer, the elastomer surface was first soaked in a solution containing an ultraviolet (UV)-assisted grafting agent. The hydrogel was then directly printed on the UV-treated elastomer by using a digital light processing (DLP) 3D printer. By comparing the intensity of the electric fields sensed by each hydrogel receiver in Figure 4C, the SAER was able to locate the relative position of the object. When wearing the SAER, the wearer receives spatial information about nearby objects in real time through auditory signals of specific frequencies generated for each of the receivers. Figure 4D shows the maximum voltage of the blue receiver corresponding to the auditory signal frequency of 0.5 kHz when the moving ball reaches the hand. By contrast, the maximum induced voltage peak of the green receiver when the hand passes the static ball corresponds to the auditory signal frequency of 1.5 kHz, as depicted in Figure 4E. This artificial electroreceptor allows a human to perceive space, a new sensory modality that does not exist in human

beings. This additional sensory mechanism could help blind or visually impaired people, who cannot rely on visual sensations, to perceive space.

Virtual reality (VR) usually involves providing audio and visual feedback to generate a virtual world in which users can interact with virtual objects[133]. In augmented reality (AR), the virtual and real worlds are combined using advanced electronics and data processing systems[134]. VR/AR devices are not directly inspired by bioreceptors, but they draw upon the human perceptual and sensory system to create immersive experiences. Figure 5A shows how perception and behaviour are shaped in response to multiple stimuli[135]. Similarly, the sensors integrated within VR/AR devices can measure physiological and body movements of a person to simulate any sensory modality of the human body. When the stimuli received by the brain match the expectations of the sensory input, the brain is more likely to treat the simulated reality as real (i.e., virtual perception) and increase engagement with the perceived illusion. For instance, Liu *et al.* developed an array of flexible and miniaturised odour generators (OGs) that can be attached to the skin above the lips[136]. These OGs were able to act as an olfaction interface wirelessly connected to the 3D virtual world and release a range of odours to enhance the realism of the VR/AR experience.

Compared to the existing VR/AR devices that provide interactive images and sounds, Yu *et al.* developed a battery-free, wirelessly controlled, and powered haptic VR interface that provided touch sensations to users[118]. This haptic interface consisted of large arrays of millimetre-scale vibratory actuators embedded in soft and conformal sheets of electronics [Figure 5B]. Multiple haptic interfaces of this type were laminated directly on several locations on the skin and controlled remotely by using a computer system. The control signals from the computer system, such as those provided through a touch screen, activated the actuators to establish VR/AR touch experiences. The interface included a large primary coil that covered the entire perimeter of the device platform to harvest adequate power to operate all the actuators. This power was passed through a linear voltage regulator to provide a fixed voltage to each actuator. Separate small near-field communication (NFC) antennas were used to independently control eight actuators through the relevant general purpose input/output (GP I/O) ports. An integrated circuit (IC) switch was associated with each actuator and transformed the fixed voltage into a square wave. To fabricate the haptic actuators, first, a copper (Cu) coil was sealed between two PDMS layers by using two moulds. A Ni-plated neodymium magnet mounted on a circular PI disk with a semi-circular slit. A PDMS ring and a silicone adhesive were used to bond the PI disk and coil together, as illustrated in Figure 5A. For the electronics part, first, a Cu layer was coated on a PI layer and patterned using photolithography and etching to form the interconnect wires, coil, and antennas. Low-temperature solder joints were formed to create electrical connections between all the other electronic components on the patterned Cu layer. An ultra-low-modulus silicone material was used as an adhesive layer between the cloth and the electronic/haptic platform. A layer of skin-coloured PDMS was used as the top encapsulation layer, which additionally provided reversible adhesion to the skin. This unique structure of the entire system facilitates scaling of the interface for various applications. Figure 5C shows an application of the VR interface. When the interface is placed on a display that shows a video feed of a girl's grandmother, the girl is able to virtually touch the hand of her grandmother through the interface. This touch on the VR interface activates the relative actuators on the VR interface mounted on the grandmother's hand, who experiences a haptic sensation with a spatio-temporal touch pattern. Other representative applications include providing tactile feedback in robotic prosthetic devices or haptic engagement in gaming.

Soft sense of touch sensor and physiological signal monitoring arrays

The sensation of touch conveys information about the objects with which we interact and about our interactions with them[6]. Touch is mediated by somatosensory neurons called mechanoreceptors embedded in the skin that relay signals from the peripheral to the central nervous system. The brain processes this

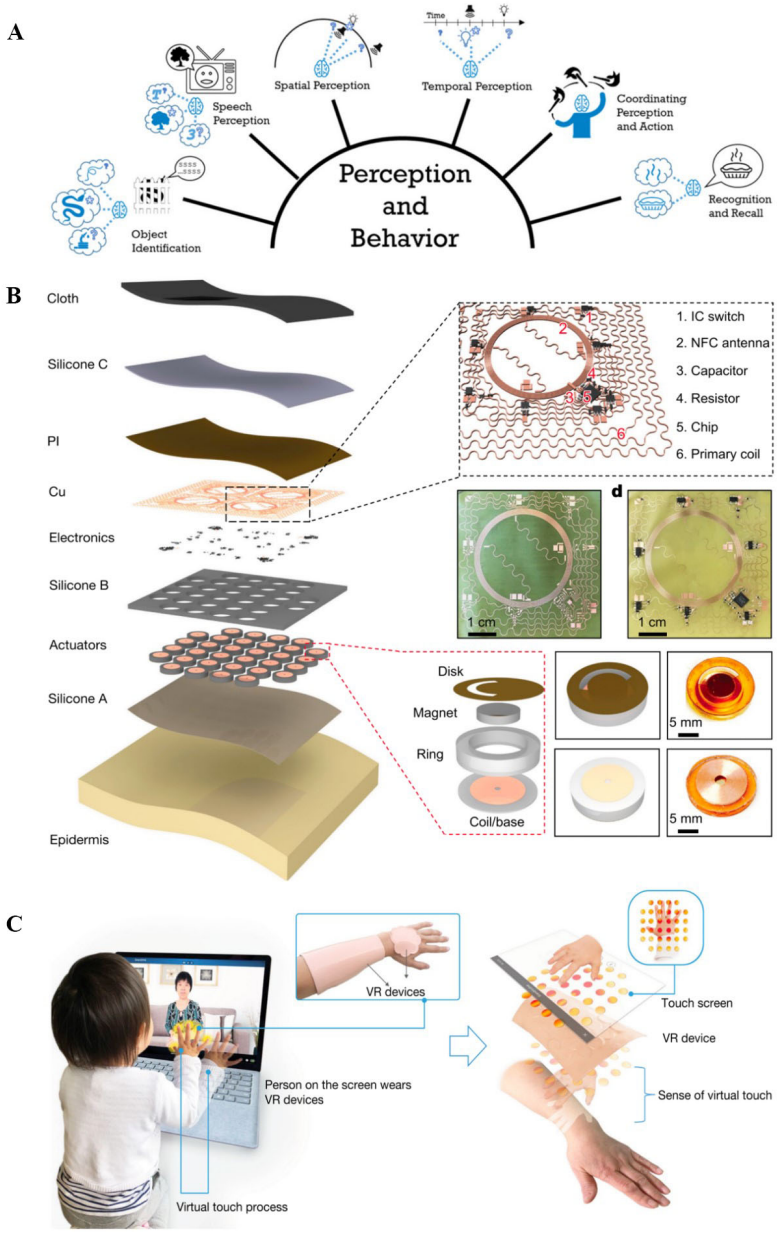

Figure 5. (A) Performance enhancement in several perceptual and behavioural domains owing to multisensory integration[135]; (B) Exploded-view schematic illustration of a device with 32 independently controlled haptic actuators, NFC electronics, circuit schematic and images, and exploded-view schematic illustration of a haptic actuator; and (C) illustration of "virtual touch process" and "sense of virtual touch" where a girl touches a screen that displays a video feed of her grandmother, who is wearing an epidermal VR device on her hand and arm. This figure is quoted with permission from Yu *et al.*[118]. NFC: Near-field communication; VR: virtual reality.

information to adjust our grasping force by engaging muscles and tendons to hold an object without crushing it. The tight coupling between the somatosensory and motor systems defines manual dexterity. The high level of dexterity of the human hand allows humans to perform numerous complex tasks. Therefore, the human hand is often used as the inspiration to develop smart skins for future interactive robotics and wearable health monitoring devices[55,137].

The human skin consists of the epidermis, dermis, and hypodermis, as shown in Figure 6A[119,138]. The hairs present within the dermis can sensitively detect environmental physical changes and transmit them to the brain through mechanoreceptors and nerve fibres.

Inspired by hairy human skin, Zhou *et al.* developed a flexible micro cilia array (MCA) layer[119]. The MCA layer worked as a dielectric layer sandwiched between two layers of Ag nanowire (Ag NW)/PDMS electrodes to form a flexible capacitive pressure sensor, as shown in Figure 6B. The MCA layer was then cut into 0.5 × 0.5 cm^2 pieces and applied as separate dielectric layers in a flexible 5 × 5 capacitive sensor array. A facile method was used to fabricate the MCA layer. First, a PDMS layer was formed on a glass substrate. Then, a layer composed of a mix of carbonyl iron particles (CIPs), PDMS, and a curing agent was spin-coated onto the cured PDMS membrane. The substrate was then moved to the surface, where the PDMS/CIP layer was magnetised using a permanent neodymium (NdFeB) magnet. This magnetic field caused aggregation of the CIPs into chains and, finally, into the cilia array patterns. The images of this sensor array in the presence of four objects of different weights and two objects having rectangular and triangular shapes are presented in Figure 6C. The detected pressure distributions and magnitudes of the four objects and the detected shapes of the rectangular and triangular objects are depicted in Figure 6C. The sensor exhibited a wide pressure detection range of 0-200 kPa with a low detectable pressure of 2 Pa. This property ensured that the sensor was suitable for a range of applications, such as real-time monitoring of elbow and finger bending, voice monitoring, wrist pulse monitoring, and pressure monitoring of the hind sole during standing, walking, and jumping. The device can be used in various applications, including wearable devices, artificial intelligence, and interactive robotics.

Inspired by mechanoreceptors and synapses[139] (i.e., the signal transmission junctions between two neurons), Kim *et al.* developed a stretchable sensory-neuromorphic system (SSNS) [Figure 7A][120]. The SSNS consisted of one 5 × 5 capacitive pressure sensor array (i.e., artificial mechanoreceptors) and four arrays (i.e., one artificial neuron), each including 5 × 5 resistive random-access memories (RRAMs) (i.e., an artificial synapse). In addition, they integrated an array of quantum dot light-emitting diodes (QLEDs) mimicking the epidermal photonic actuators that exist on golden tortoise beetles to display the output signals of the pressure sensor array. The usage of intrinsically stretchable printed interconnects between these components stabilised the operation of the system under up to 25% stretching, which is similar to the range of skin deformation. To fabricate the pressure sensor array, a sinter-free ink was prepared by mixing the polymer [PDMS-(4,4′-methylenebis(phenyl isocyanate) (MPU)0.4-isophorone diisocyanate (IU)0.6] with methyl isobutyl ketone (MIBK) and Ag flakes. The ink was screen-printed using a metal screen mask to pattern the bottom and top electrode layers of the capacitive sensors. Moreover, the dielectric layer was screen-patterned using a metal screen mask. RRAMs consisting of layers of patterned PI, Au/Al, titanium dioxide (TiO_2), Al/Au, and the final SU8 encapsulation layer were fabricated on a SiO_2 wafer. A thermal release tape was used to detach PRAMs from the SiO_2 wafer and transfer them onto a PDMS substrate. The sinter-free ink was used at the end to pattern the interconnects by means of screen printing. A similar fabrication method was used to fabricate QLEDs. The fabrication process consisted of patterning islands of PI, Ag/Au, zinc oxide (ZnO) nanoparticles, and red-emitting cadmium selenide/cadmium zinc sulphide (CdSe/CdZnS) quantum dots on a SiO_2 wafer. The islands were transferred onto a PDMS substrate by using a thermal release tape. This step was followed by thermal evaporation of a hole-transport layer (HTL), a hole-injection layer (HIL), an Ag layer as the anode, and a final SiO_2 encapsulation layer. The interconnects were then screen-printed. Figure 7B shows the system receiving four types of patterned stimuli (“S”, “N”, “U”, and “K”) through a 5 × 5 capacitive pressure sensor array. The output of the capacitive sensor array with and without 25% stretching is depicted in Figure 7C. The outputs of 25 capacitive sensors were converted to voltage signals and applied to the four RRAM arrays, shaping an artificial neural network

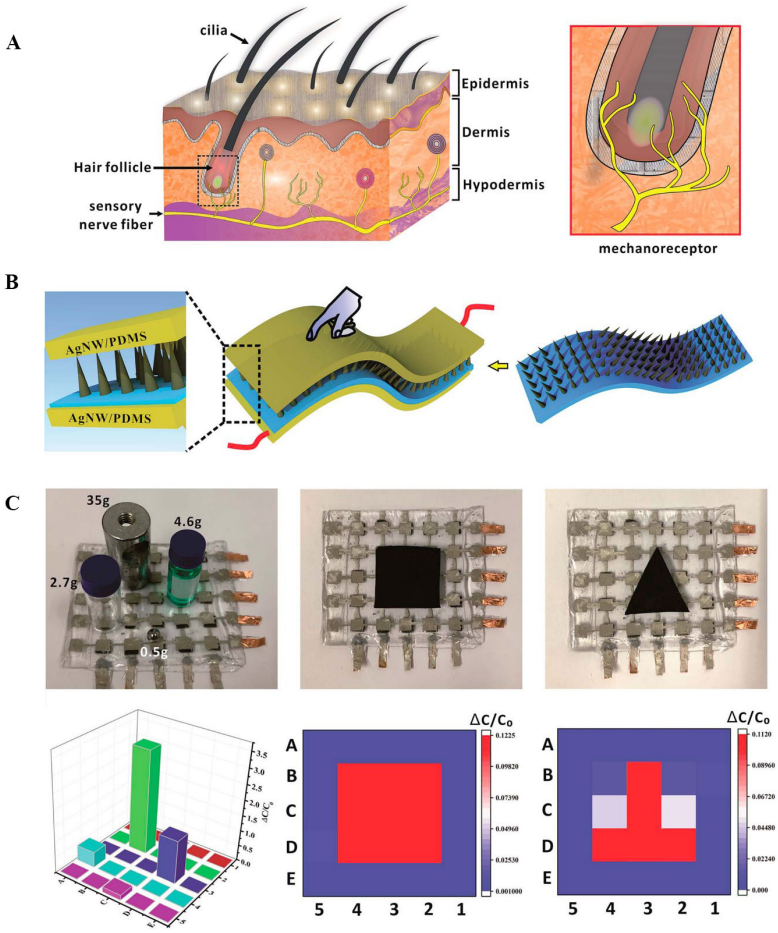

Figure 6. (A) Schematic illustration of the human skin and its hair-sensing mechanism; (B) the schematic illustration of capacitive pressure sensor with MCA as the dielectric layer; and (C) optical images of sensor arrays for pressure detection from different objects of various weights and shapes, and the related pressure distribution readouts. This figure is quoted with permission from Zhou *et al.*[119]. Ag NW: Ag nanowire; MCA: micro cilia array; PDMS: polydimethylsiloxane.

(ANN). Two different neural networks were employed and trained for un-stretched and 25%-stretched RRAM synapses to classify the input patterns. The output results were then applied to the 5 × 5 QLED arrays to visualise the "S", "N", "U", and "K" patterns formed by the QLED [Figure 7D]. The bioinspired SSNS can be used in applications such as smart skin prosthetic systems.

Pulse and respiration are two vital signals that provide an accurate assessment of individual health status[140]. For effective detection of these subtle signals through the skin, soft and flexible wearable devices are required that could mimic the electrical properties and softness of human skin.

Wang *et al.* developed a flexible and wearable 3 × 3 pulse monitoring pressure sensor array that can acquire 3D pulse signals at three pulse positions called Chi, Cun, and Guan on the radial artery [Figure 8A][121]. These positions are important in palpation-based pulse diagnosis in traditional Chinese medical science (TCMS). The array was composed of resistive pressure sensors that converted the pulse signals of the artery to resistance changes, and the results were fed to a data acquisition system. A pre-processing circuit converted the resistance signals to voltage signals and amplified them; the amplified signals were subjected to noise filtering to remove high-frequency noise. Then, ADC conversion was applied to the multichannel

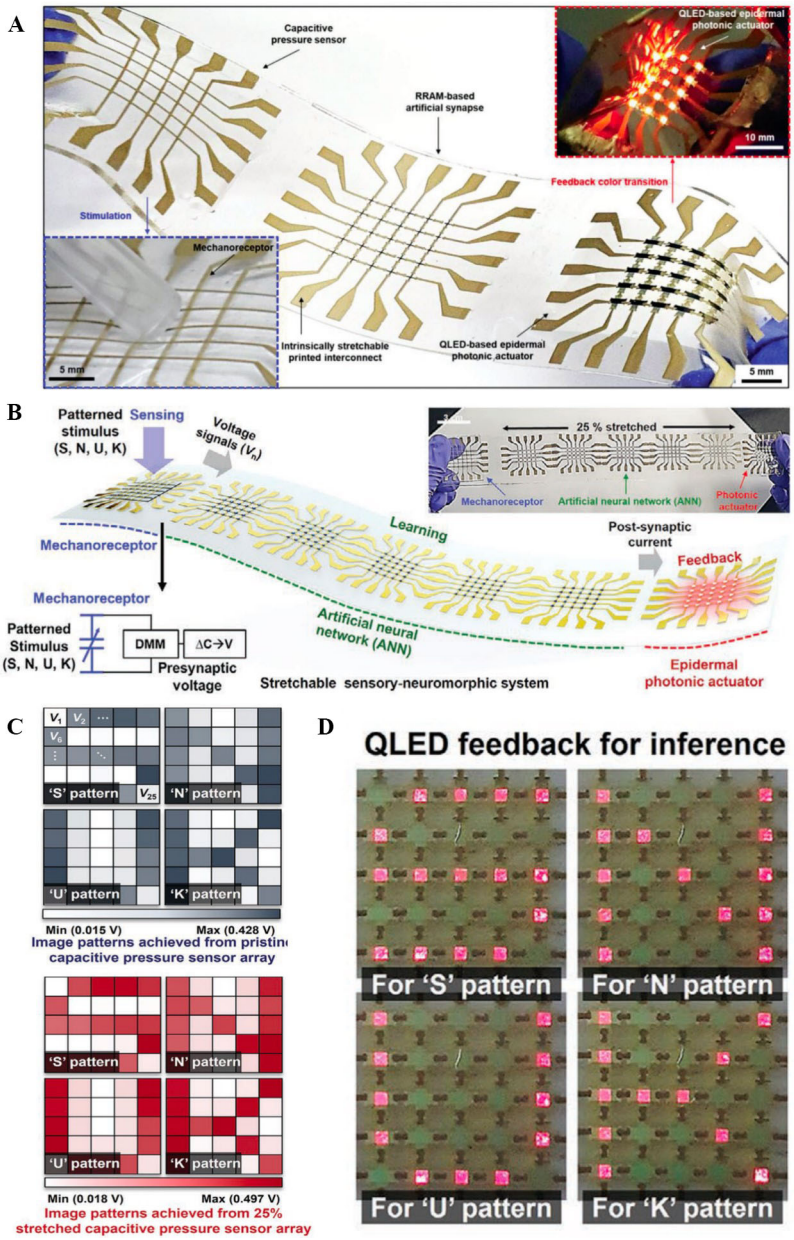

Figure 7. (A) Photograph of a stretchable sensory-neuromorphic system; (B) schematic illustration and image of SSNS and its overall operation; (C) image patterns ("S", "N", "U", and "K") provided by the pristine (top) and 25%-stretched (bottom) mechanoreceptors; and (D) photographs of epidermal photonic actuator array visualising the trained/inferred patterns of "S", "N", "U", and "K". This figure is quoted with permission from Kim *et al.*[120]. QLED: Quantum dot light-emitting diode.

pulse signals to construct a 3D map based on a polynomial fitting equation. A schematic illustration of this pulse sensing platform is presented in Figure 8A. The IDEs of each pressure sensor were screen-printed on a PET substrate by using a conductive Ag paste. A PDMS mould was prepared using a 3D-printed mould to define the sensing layers of the sensors above the IDEs. The PDMS mould and PET layer were bonded, and an ion gel layer was coated as the sensing layer through the PDMS mould above the electrodes. The device was then encapsulated with an ecoflex layer. The pulse signals (i.e., pulse strength versus time) recorded using nine pressure sensors are depicted in Figure 8B. The distance between two valleys (i.e., shown in yellow) defines the response time for one cardiac cycle. The three peaks in each cycle present the early

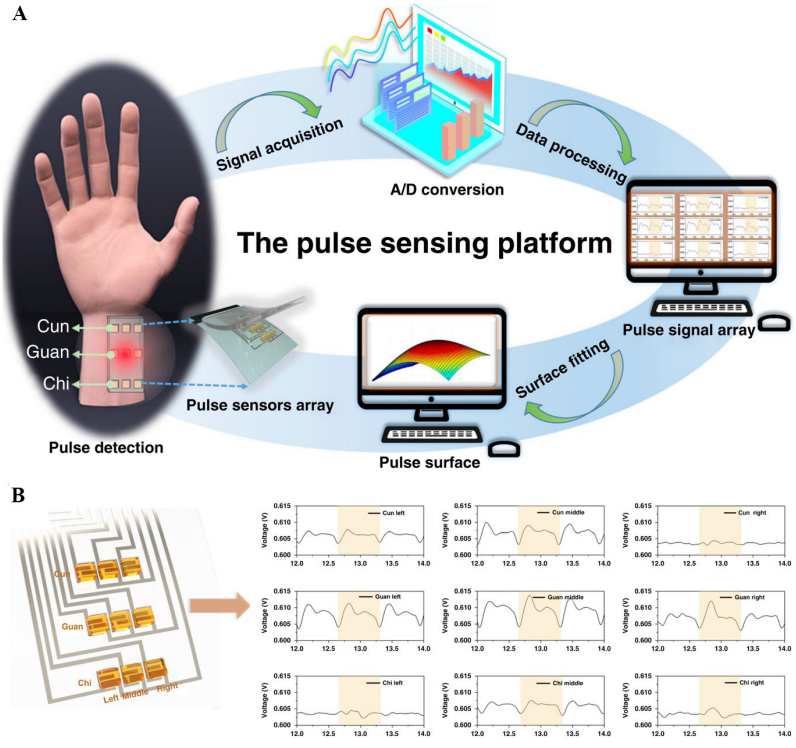

Figure 8. (A) Schematic illustration of the pulse-sensing platform comprising sensor arrays, signal processing, signal display, and 3D signal fitting; and (B) corresponding pulse signals (Cun, Guan, and Chi) detected by the nine sensor arrays[121].

systolic peak (P_1), inflexion point (P_2), and dicrotic peak (P_3). The similar peaks and valleys of all the waveforms indicate good synchronisation in the multichannel acquisition system. This pulse monitoring device can modernise Chinese medical science or be used in intelligent healthcare applications.

A triboelectric all-textile sensor array (TATSA) developed by Fan *et al.* can be stitched to clothes as a wristband, fingerstall, sock, and chest strap[122]. TATSA was used to monitor arterial pulse waves and respiratory signals from various parts of the body. The physiological signals by TATSA recorded were amplified, low-pass-filtered, passed through an ADC converter, and transmitted wirelessly through Bluetooth to a mobile application for health status analysis [Figure 9A]. TATSA was knitted with conductive and commercial nylon yarns to prepare a full cardigan stitch [Figure 9B]. To prepare the conductive yarn, stainless-steel wires were twisted with several commercial terylene yarns. When an external force was applied and the two yarns came into contact with each other, equivalent charges with opposite polarities were generated on the surface of the two yarns because of triboelectrification. Once the two yarns separated, positive charges were induced in the inner stainless steel because of the electrostatic induction effect. The process of charge transfer during this contact–separation movement is presented in Figure 9C. The pulse waves recorded from the TATSA positioned at various points on the body of a 25-year-old woman are shown in Figure 9D. Three distinguishable peaks (P_1 to P_3) are visible on the pulse waveforms recorded at the neck, wrist, and fingertip positions, but the ankle waveform does not exhibit the P_2 peak. Figure 9E shows the positioning of TATSA on the chest for monitoring respiration. The detected waveform is the superimposition of the respiratory and heartbeat waveforms. A 0.8 Hz low-pass filter and a 0.8-20 Hz band-pass filter were used to separate the signals, as shown in Figure 9E. The sensor array could be used for long-term and non-invasive assessments of cardiovascular disease and sleep apnoea syndrome.

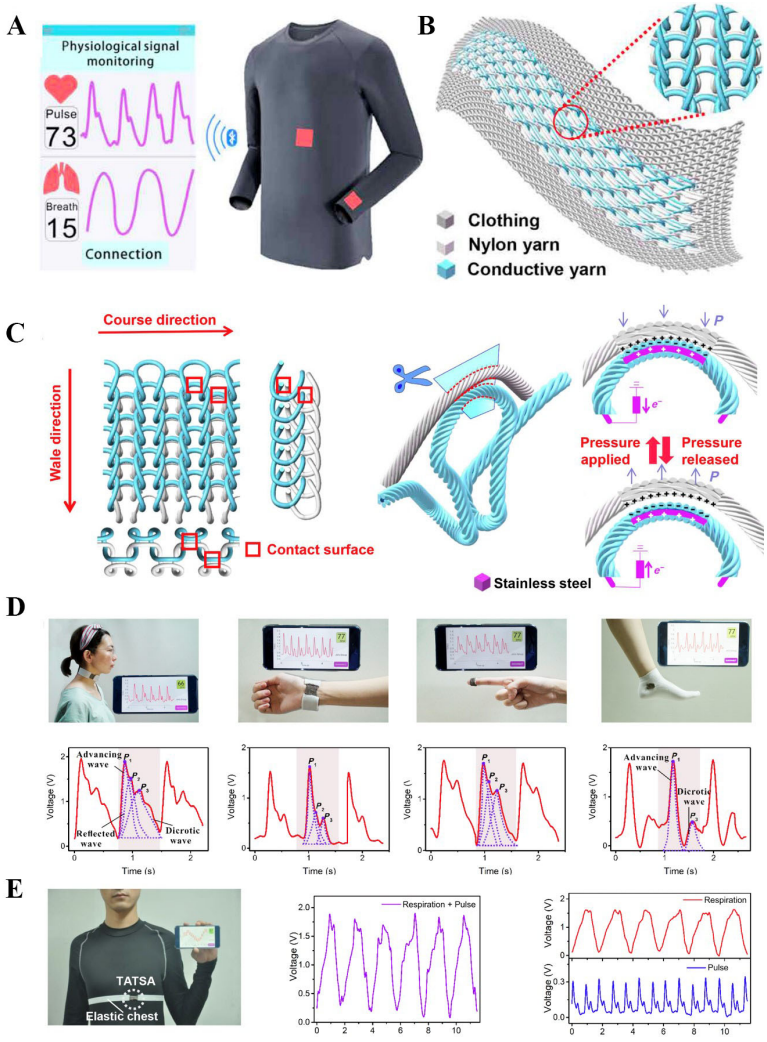

Figure 9. (A) Two TATSAs integrated into a shirt for real-time monitoring of pulse and respiratory signals; (B) schematic illustration of the combination of TATSA and clothes; (C) TATSA with the front, right, and top sides of the knit loops, and schematic illustrations of charge transfer through a contact unit during the pressure application and release steps; (D) photographs of TATSAs stitched into a wristband, fingerstall, sock, and chest strap, and the related measured waveforms; and (E) TATSA placed on the chest for measuring respiration signals, and the detected voltage-time and its decomposition into the heartbeat and respiratory waveforms[122]. TATSA: Triboelectric all-textile sensor array.

Soft tongue stimulation electrode and tasting arrays

A tongue is a soft, flexible, and sensitive muscular organ with taste buds that include thousands of mechanical and taste receptors, as well as ion channels[141]. The development of flexible electrode arrays for electrical stimulation of the tongue has facilitated investigation into a brain-tongue-machine interface from the perspective of the development of clinical neuromodulation and tissue-activation techniques. The five tastes experienced by mammals and humans are sweet, bitter, sour, salty, and umami. The recognition of sweet, bitter, and umami tastes is generally attributed to taste receptor cells (TRCs), whereas the recognition of sour and salty tastes is attributed to specific membrane channels on TRCs. This indicates that the sensing intensities of all five tastes rely on the distribution of tastebuds rather than the taste map shown in Figure 10A. In addition to chemically induced tastes, electrical stimulation can induce taste sensations.

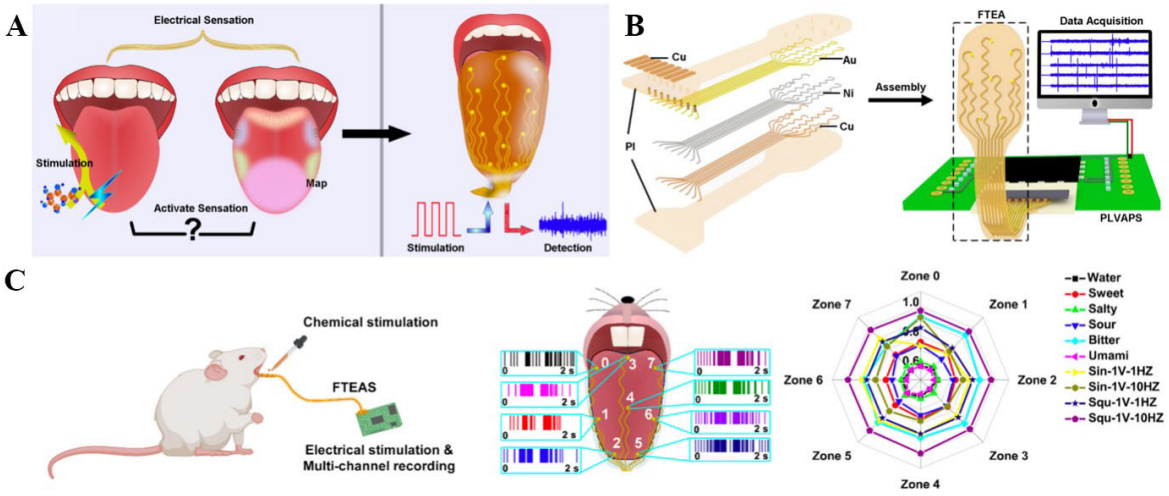

Figure 10. (A) Schematics of electrical and chemical activation of some senses on the tongue (left) to determine whether the taste was related to the distribution of taste bud zones (middle), and the FTEAS device developed to electrically stimulate the tongue and detect activated cell-firing-related signals from each zone of the tongue simultaneously; (B) exploded-view schematic of FTEAS, and schematic of FTEAS showing FTEA, PLVAPS, and the data-acquisition module; (C) schematic illustration of the rat *in vivo* experiments, spike signals recorded from eight zones of the rat's tongue, and zone-distribution radar map of the spike counts induced by chemical and electrical stimulations. This figure is quoted with permission from Huang *et al.*[123]. FTEAS: Flexible tongue electrode array system; PLVAPS: portable low-voltage adjustable power supply.

Huang *et al.* developed a flexible tongue electrode array system (FTEAS) to electrically stimulate different regions of the tongue and collect multisite signals from the tongue [Figure 10A][123]. Figure 10B shows the layers of the FTEAS and a portable low-voltage adjustable power supply (PLVAPS)-stimulating module that was fabricated on a custom-designed PCB. The data acquisition module was responsible for collecting electrical signals from the FTEAS. The main power supply of the system was a 5 V DC battery. To fabricate the FTEAS, first, the Au/Ni/Cu electrodes and wiring were patterned onto a thin PI substrate. Then, another PI film with small holes above the Au/Ni/Cu electrodes was laminated to encapsulate the device. The results of simultaneous electrical stimulation of eight zones of a rat tongue are shown in Figure 10C. The recorded spike signal counts in each zone were summarised as the radar map. All spikes were normalised to the maximum counts recorded in Zone 4, which was induced by the 1 V, 10 Hz square wave stimulation signal. A similar number of spikes were observed for each chemical taste stimulation in all zones. The sinusoidal wave-induced spikes showed divergence in terms of spike counts in Zones 0 and 1. By contrast, symmetric spikes were obtained by the square-wave stimulations, similar to the case of chemical taste stimulations. Non-invasive electrotherapy for neurological diseases through the tongue and a tongue-machine interface is a potential application of FTEAS.

The tactile receptors (i.e., low-threshold mechanoreceptors) on the surface of the tongue are responsive to stimuli evoked by physical contact between the tip of the tongue, food, tooth, and lip[142]. A few research studies have focused on oral somatosensation, which has not been understood very well thus far. For instance, an array of flexible electrode arrays has been developed to stimulate the dorsal surface of the tongue[143]. This array can be used to evoke lost senses, such as vision, audition, proprioception, and the vestibular senses.

Inspired by the astringency perception mechanism of the human tongue upon licking a liquid [Figure 11A], Yeom *et al.* developed a soft hydrogel-based artificial tongue that mimics the thin salivary layer of the tongue[124]. Unlike the previously developed artificial tongues, which require large amounts of liquid for operation, trace amounts of analytes are sufficient for detection with this device. This artificial tongue consists of a 3 × 3 sensor array with a saliva-like hydrogel acting as the sensing layer. The hydrogel consists

of mucin as a secreted protein, lithium chloride (LiCl) as an electrolyte, and polyacrylamide (PAAm) as the 3D porous polymer network to facilitate facile electrolyte flow, as illustrated in Figure 11B. Additionally, a tannic acid (TA) solution was used to prepare the hydrogel layer because it could induce the formation of

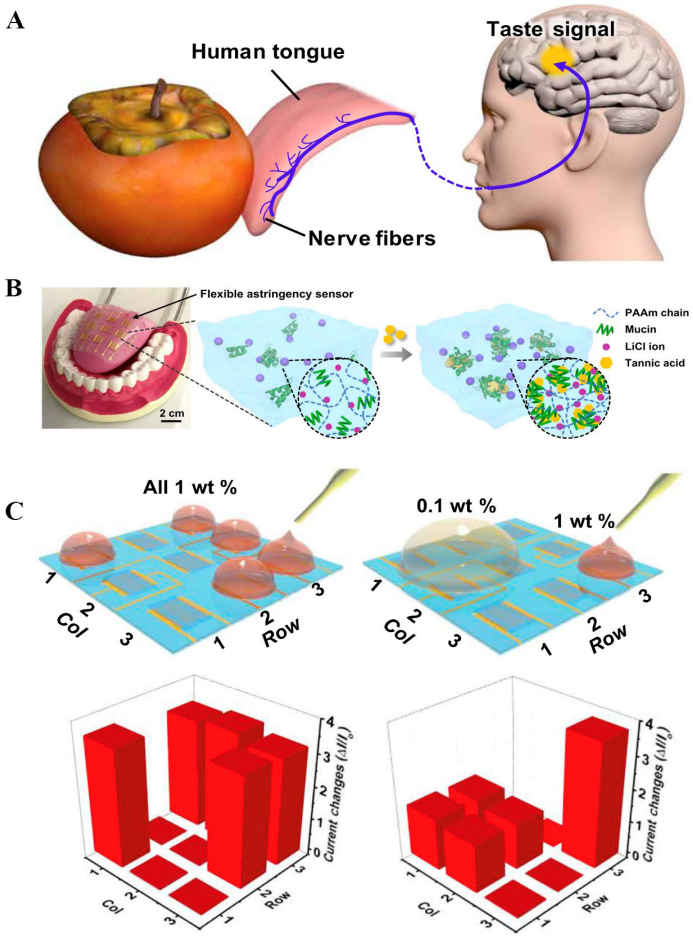

Figure 11. (A) Schematic illustration of wipe-and-detection of the human tongue; (B) an image of the artificial tongue and schematic illustration of the astringency-sensing principle of the artificial tongue; and (C) application of five drops of 1 wt.% TA to the artificial tongue array (left panel) and two drops of 0.1 and 1 wt.% TA to the array (right panel), along with the corresponding taste mapping data[124]. TA: Tannic acid.

hydrophobic aggregates and enhance ionic conductivity. Direct UV polymerisation of the hydrogel on a poly(ethylene naphthalate) (PEN) substrate with patterned Au IDEs was realised using 3-(trimethoxysilyl)propyl methacrylate (TMSPMA) as the chemical anchoring agent. When 0.1 and 1 wt.% TA solutions were applied at five different spots on the array, the sensor measured the corresponding current changes to generate taste maps [Figure 11C]. The largest current changes were observed at the spots where 1 wt.% solution was applied, whereas the spots where 0.1 wt.% solution was applied exhibited smaller current changes. This artificial tongue could be used as a platform for future applications involving portable taste-monitoring devices and humanoid robots.

Soft odour identification sensor arrays

The human olfactory system is responsible for our sense of smell. The nose houses various receptor families that detect volatile chemical stimuli which dissolve in the mucus lining[144]. The action potentials generated in the receptors travel along their axons, which terminate in the olfactory bulb. The olfactory information then travels to the olfactory cortex for processing, as shown in Figure 12A[145]. The electric nose (e-nose) that could mimic this operation could include an array of chemical sensors, electronic circuitry (e.g., sampling, filtering, and signal conditioning), and data analysis software [Figure 12A][145].

Lorwongtragool *et al.* developed a wearable e-nose by integrating a 4 × 2 chemical sensor array with a Zigbee wireless communication system [Figure 12B][125]. The sensor array comprised eight fully inkjet-printed gas sensors on a PEN film with Ag ink IDEs. The resistance of each sensor was determined by connecting it to a voltage divider. The output voltages of eight sensors were then applied to an eight-channel analogue multiplexer connected to a USB data acquisition (DAQ) device. To fabricate the sensing layers of sensors 1-4, layers of a multi-walled CNT (MWCNT) solution were inkjet-printed on electrodes, followed by the printing of a polymer layer composed of one of the following polymers: polyvinyl chloride (PVC), poly(styrene-co-maleic anhydride), cumene terminated poly(styrene-co-maleic anhydride) (Cumene-PSMA), polysulphone (PSE), and polyvinylpyrrolidone (PVP). For sensors 5-8, each polymer was blended with the MWCNT solution and printed on electrodes. The sensor array was exposed to four individual volatile organic compounds (VOCs) present in the volatiles released from the axillary skin. The sensor response percentages for the four VOCs are shown in Figure 12C. The e-nose was used to monitor the body odour of a participant before exercise, after exercise, and after relaxing for a long period post-exercise. The data were collected for 5 min in each step, and the entire data-collection process was repeated thrice. Principal component analysis (PCA) based on unsupervised learning was used to observe the odour progression in each minute and classify the odour of the armpit when performing different activities. This wearable e-nose could be used to detect unusual odours corresponding to various health statuses.

Zheng *et al.* developed a skin odour detection sensor array (i.e., e-nose system) consisting of 3 × 2 sensors based on CNTs and polymer suspension solutions as the sensing materials[126]. This flexible sensor array data was read using a voltage divider circuit and interfaced with an MCU for data acquisition. A Bluetooth chip and a button cell were used for wireless transmission and as the power supply, respectively [Figure 13A]. To prepare the sensing material solutions, one of the three polymers [hydroxypropyl methylcellulose (HPMC), poly(methyl vinyl ether-co-maleic anhydride) (PMVEMA), and polyvinyl pyrrolidone (PVP)] was mixed with carboxylated or hydroxylated CNTs by ball milling. Ag IDEs were screen-printed on a PET substrate. Then, 5 μL of the sensing solution was drop-casted on the respective electrodes and dried. To avoid direct contact with sweat, a hydrophobic and breathable PVDF membrane was laminated onto the sensor array. A schematic of the wearable e-nose system integrated into an armband is shown in Figure 13B. The sensor was placed under the armpit, while the related circuitry was placed on the bicep. The responses of each sensor to 5-25 ppm of hexanoic acid, dodecane, and decanal (i.e., elements with an odour similar to sweat) were measured to calculate their sensitivities [Figure 13C]. The e-nose system was tested on eight participants while they walked for 63 min on a treadmill. The experiment was repeated on four consecutive days. The responses of the sensors were then used for feature extraction, and a K-means clustering algorithm was applied to identify human odour. This e-nose system that can detect human skin odour can be used for individual identification or to determine individual physiological status.

Soft sound sensor arrays

Sound energy is conveyed by the pinna and auditory canal to the eardrum[146,147]. Vibrations of the eardrum are amplified and transmitted by the middle ear bones, namely, the malleus, incus, and stapes, to the inner ear fluid. The cochlea is a fluid-filled duct in the inner ear that is responsible for converting sound

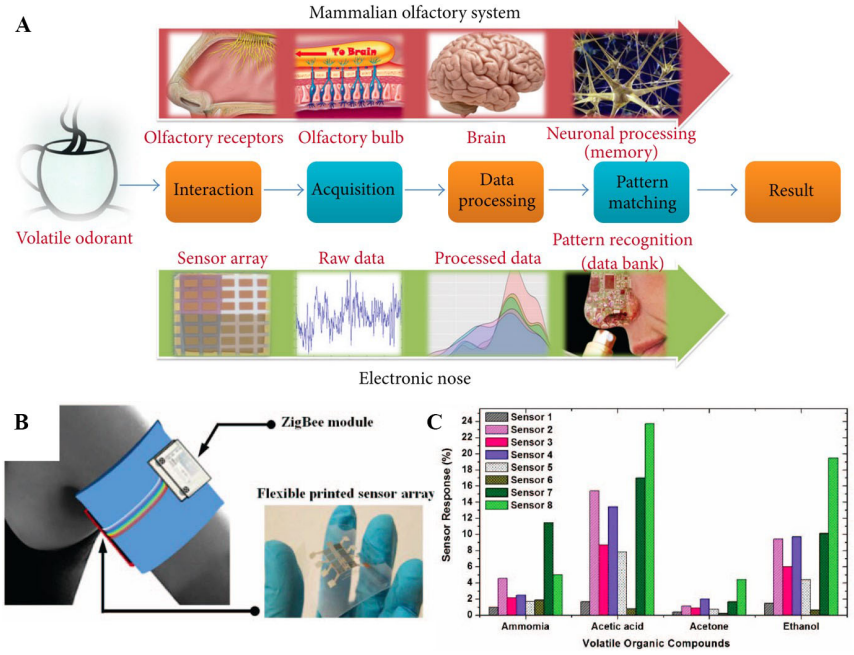

Figure 12. (A) Schematic illustration comparing the mammalian olfactory system with an electronic nose (e-nose)[145]; (B) Schematic illustration of wearable e-nose with the ZigBee module and a photo of the fabricated e-nose sensor array; and (C) sensor array exposed to 200 ppm of volatiles, namely ammonia, acetic acid, acetone, and ethanol. This figure is quoted with permission from Lorwongtragool *et al.*[125].

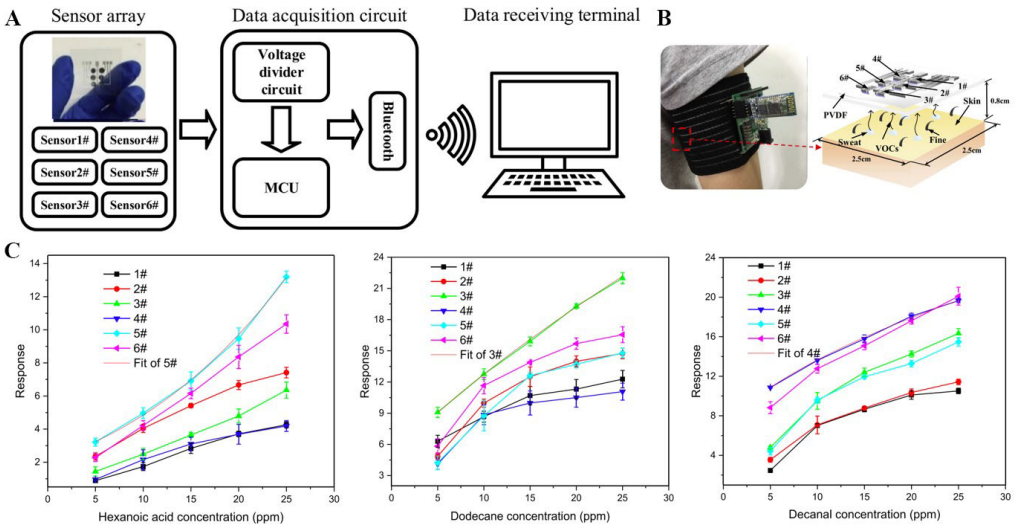

Figure 13. (A) Schematic illustration of the working principle of the wearable e-nose system; (B) photograph of a wearable e-nose on the armpit of a subject, with an integrated chemical sensor array and wireless circuit; and (C) responses of the sensor array to 5-25 ppm of hexanoic acid, dodecane, and decanal. This figure is quoted with permission from Zheng *et al.*[126]. MCU: Micro-controller unit; PVDF: poly(vinylidene fluoride); VOCs: volatile organic compounds.

vibrations into electrical signals with the help of specialised sensory cells. These electrical signals are then transmitted to the brain through the auditory nerve for processing. The structure of the human ear is shown in Figure 14A[146].

Yang *et al.* developed a 3 × 3 array of self-powered acoustic sensors based on a piezoelectric poly(vinylidene fluoride-trifluoroethylene) [P(VDF-TrFE)] thin film (PTF) [i.e., P(VDF-TrFE) acoustic sensor (PTAS) array] that was integrated with a 3D-printed bionic ear[127]. The PTF layer converted the mechanical vibration of sound waves to electric signals, similar to the eardrum and cochlea. Data-acquisition cards and circuits were developed to collect and transmit electrical signals to the processing

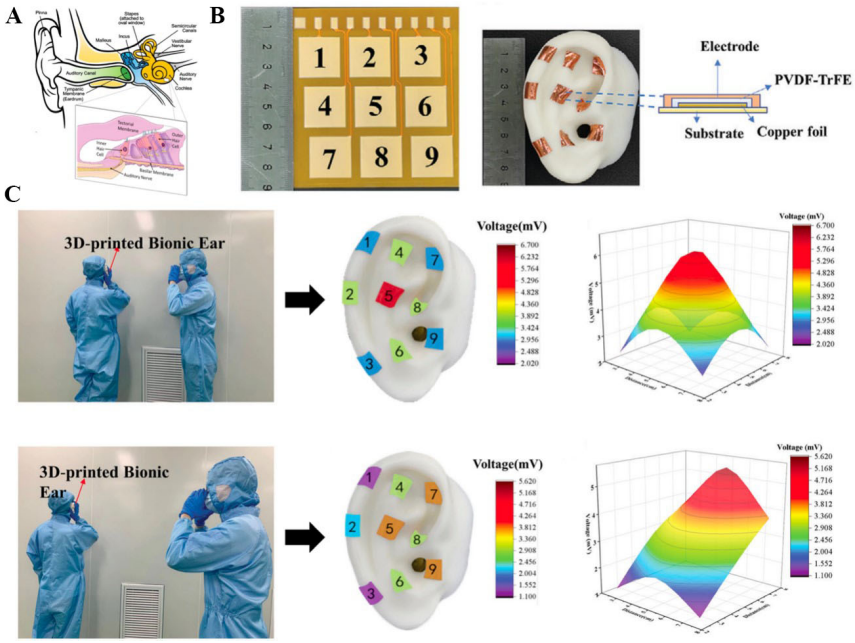

Figure 14. (A) Structure of the human ear[146]; (B) Nine different modules of the FPC and an optical image of the PTAS; (C) piezoelectric voltage distribution of the array on the 3D ear, and 3D sound diagrams of the cases in which the sound source was placed above pixel 5 (top) and pixel 8 (bottom). This figure is quoted with permission from Yang *et al.*[127]. PTAS: P(VDF-TrFE) acoustic sensor; PVDF-TrFE: poly(vinylidene fluoride-trifluoroethylene).

computer, similar to the nerve cells. To fabricate the PTAS array, P(VDF-TrFE) powder was dissolved in methyl ethyl ketone, and the solution was stirred magnetically. Thereafter, the solution was coated on an FPCB and placed in a vacuum chamber to form a PTF film, which was then annealed. The annealed PTF film was then polarised *in situ*. Afterwards, a Cu foil layer was pasted on top of the film. Finally, the resulting flexible circuit was attached to a 3D-printed ear, as shown in Figure 14B. The 3D-printed ear was used to map sound waves from two different sound sources at two different locations [Figure 14C]. The piezoelectric voltage of each pixel was then collected, and a corresponding colour-scaled 3D diagram was simulated based on the acquired piezoelectric signals. When the sound source was directly opposite the 3D-printed ear, pixel 5 exhibited the highest piezoelectric response of 6.232 mV because it was the nearest to the sound source. When the sound source was located diagonally opposite to the 3D-printed ear, pixel 8 exhibited the highest piezoelectric voltage of 5.612 mV because it was the nearest to the sound source. This PTAS array can be used for sound identification and localisation in bionic applications.

MULTIMODAL SOFT SENSOR ARRAYS

It is possible to develop a simple artificial somatosensory system or personalised diagnostic system by realising simultaneous detection of multiple stimuli with a single device or system[148-157]. Such multimodal sensors reported in the literature can be divided into two types: sensors that merge different sensing principles or sensors that spatially integrate different sensing elements[128,129,158-161]. Here, one example of a sensor from each category is provided.

Inspired by the epidermal-dermal microstructure of human skin, Shin *et al.* demonstrated a self-powered sensor array based on an interlocked ferroelectric copolymer P(VDF-TrFE) microstructure that can simultaneously detect temperature and pressure, as shown in Figure 15A[128]. The two layers of the P(VDF-TrFE) microstructure were inversely polarised with polarity concentration in the area around the microstructures. This concentration and the spacer effect of the interlocked micro-ridge structures

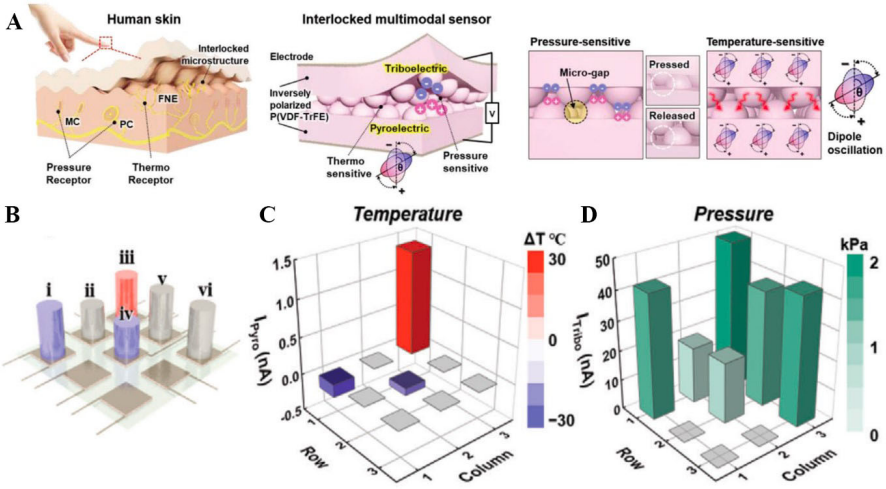

Figure 15. (A) Schematics of human skin and the interlocked multimodal sensor used for pressure and temperature sensing because of its structural advantages; (B) schematic illustration of the 3 × 3 device used to detect different objects with various temperatures and pressures: (i) 2 kPa at ΔT (temperature change) -30 °C, (ii) 1 kPa at room temperature, (iii) 2 kPa at ΔT 30 °C, (iv) 1kPa at ΔT -30 °C, and (v), (vi) 2 kPa at room temperature; (C) detected temperature; and (D) pressure profiles of objects i-vi by using the sensor array[128]. PC: Personal computer.

enhanced the triboelectric output performance of the device. The triboelectric effect was used to detect pressure changes, while the pyroelectric response of the P(VDF-TrFE) microstructure was used to detect temperature changes. Pyroelectric materials are naturally electrically polarised and have large internal electric fields. When these materials are heated or cooled, a temporary voltage is generated (i.e., pyroelectricity)[162]. A 3 × 3 sensor array composed of P(VDF-TrFE) microstructures was fabricated with top and bottom Al electrodes, as illustrated in Figure 15B. Objects (i-vi) of different weights and temperatures were placed on the sensor array. The triboelectric and pyroelectric output signals corresponding to the applied pressures and temperatures, respectively, were measured simultaneously. Maps of the output signals versus temperature and pressure are shown in Figure 15C and D, respectively. These results indicate a correct correlation between the output pyroelectric and triboelectric currents and the applied temperature and pressure inputs, respectively. This P(VDF-TrFE) sensor array can be used as a self-powered and multimodal sensor in the healthcare, environmental monitoring, security, and human-machine interface domains.

Hua *et al.* developed a skin-inspired stretchable and conformable matrix network (SCMN) for multifunctional sensing of temperature, in-plane strain, humidity, light, magnetic field, pressure, and proximity [Figure 16A][129]. The multi-layered design layout is depicted in Figure 16B. The SCMN was composed of 100 sensory nodes connected with meandering wires, and various sensors were positioned on different nodes. To fabricate the SCMN, first, a PI layer was coated on a poly(methyl methacrylate) (PMMA)-coated silicon substrate. A few photolithography steps were performed to pattern the meandering wires, electrodes, and sensors on the nodes. Then, a PI encapsulation layer was coated on the sensors. A lift-off process was executed to pattern a SiO_2 hard mask on the meandering connections and nodes, followed by reactive-ion etching the remainder of the PI layer. The remaining layer, namely, a stretchable network, was then released from the silicon wafer and transferred to a piece of poly(vinyl alcohol) (PVA) or PDMS. An Ag thin film was sputtered on the opposite side of the etched network to form the bottom and top electrodes, along with an ecoflex silicone elastomer dielectric to form the pressure and proximity sensors on a few nodes. The materials used to fabricate the sensors included Pt for the resistive temperature sensor, constantan for the in-plane strain sensor, Al/PI for the humidity sensor, Al/ZnO for the UV light sensor, and cobalt (Co)/Cu multilayer for the magnetic field sensor. The sensor measurement results are presented

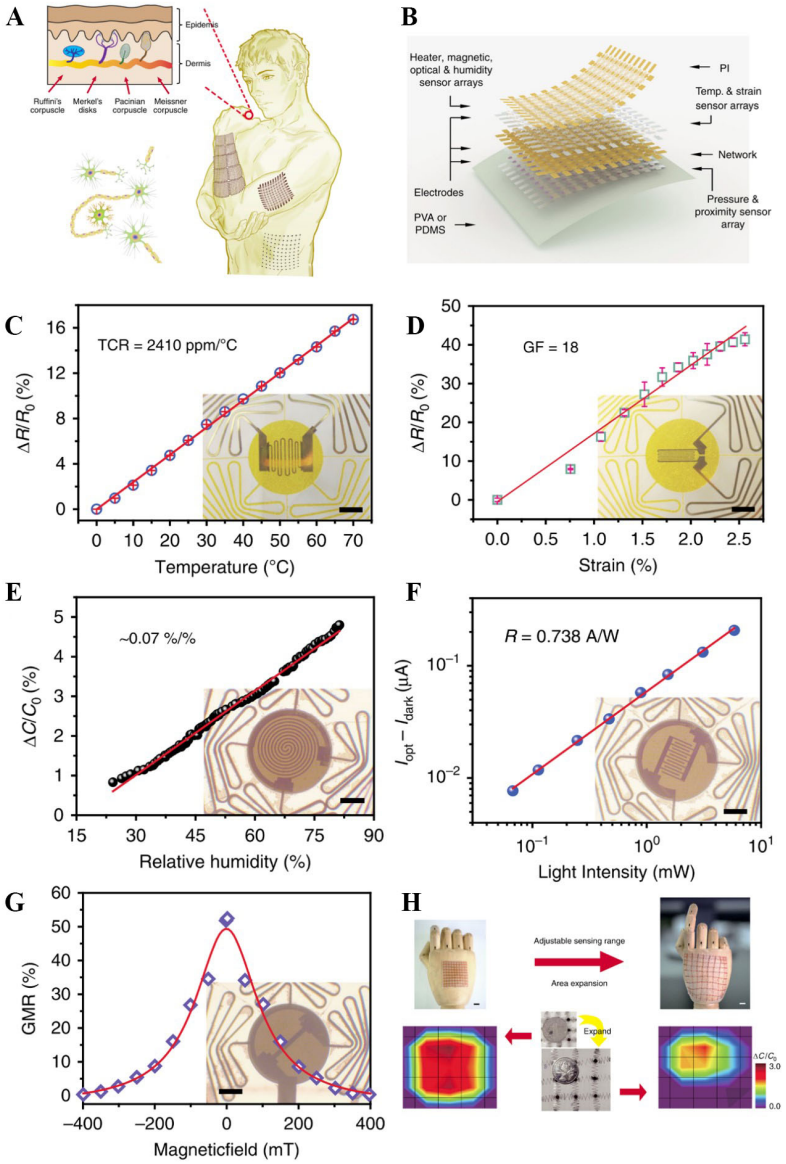

Figure 16. (A) Schematic illustration of SCMN on a human arm, and an expanded network (expansion: 200%) on a human abdomen (right); tree branch-like neuron connections (left bottom); and sensory receptors of the glabrous skin (left top); (B) exploded-view schematic of an SCMN with eight functions (temp.: temperature); (C) temperature sensing; (D) in-plane strain sensing; (E) humidity sensing; (F) light sensing; (G) magnetic sensing responses; and (H) pressure mapping before and after 300% expansion of an SCMN placed as an artificial skin on a hand[129]. GF: Gauge factor; GMR: high magneto-resistive; PDMS: polydimethylsiloxane; PI: polyimide; PVA: poly(vinyl alcohol); SCMN: stretchable and conformable matrix network; TCR: temperature coefficient of resistance.

in Figures 16C-G. The relative resistance of the temperature sensor changed linearly in the temperature range of 0-70 °C with a temperature coefficient of resistance (TCR) of 2,410 ppm/°C for Pt [Figure 16C]. The relative change of resistance of the in-plane strain sensor was linearly correlated to the applied strain, leading to a high gauge factor (GF) of 18 [Figure 16D]. In the case of the humidity sensor, the absorption of water molecules changed the permittivity of PI and, thus, the capacitance of the humidity sensor, yielding a linear correlation between change in capacitance and relative humidity (RH) with a slope of 0.07 [Figure 16E]. The UV light sensors exhibited a fast photoresponsivity (R) of 0.738 A/W [Figure 16F]. The magnetic field sensor achieved a high magneto-resistive (GMR) ratio of 50% [Figure 16G]. Figure 16H

demonstrates the SCMN attached as an artificial skin onto a wooden hand with and without sensing area expansion. This demonstration proved the adjustability and expandability of the system. In addition, the SCMN exhibited stable performance under 300% expansion, as shown in the pressure mappings obtained under an applied pressure load. The SCMN could be in applications related to health monitoring, humanoid robotics and prosthetics, and human-machine interfaces.

CONCLUSION AND FURTHER PERSPECTIVES

The use of single sensors that can detect bio-signals in healthcare applications leads to false-positive or negative results[163]. Drawing inspiration from the multitude of bioreceptors that occur naturally in groups of millions within the body, soft sensor arrays have been developed to provide much more meaningful, robust, and reliable results. However, the development of flexible, stretchable, and conformable sensor arrays requires careful selection of durable and biocompatible materials[164,165]. When improving the flexibility and stretchability of these arrays, one should not compromise their sensitivity and resolution[81,166]. Adhesion, biodegradability, permeability, and water repellence are the other material factors that should be considered based on the target application[167]. The manufacturing techniques used to fabricate these arrays should be scalable, cost-effective, and reliable to facilitate their widespread adoption in various applications[168,169]. The development of sensors in the array format provides high spatial resolution, but crosstalk and interference between sensors should be avoided to ensure accurate signal detection[170]. Moreover, the signals obtained using sensor arrays may contain abundant information from untargeted stimuli, and therefore, it is critical to decouple this interference[171]. To ensure long-term detection stability of sensor arrays under complex application conditions, one must carefully select suitable encapsulation materials, forms, and methods, an area that warrants further investigation[172]. The interfacing of soft arrays with rigid electronics is another challenge that calls for the development of flexible and compatible interconnects[173].

The complex signals recorded by sensor arrays often necessitate the use of advanced algorithms and machine learning (ML) techniques to realise real-time signal processing, noise reduction, and data interpretation[174,175]. The selection of appropriate algorithms to process different types of raw data is critical to achieve a correct and robust outcome. For instance, to identify various objects using a pressure sensor array, a multilayer perceptron (MLP) (i.e., a class of ANNs) can be used. MLP is effective for classification without explicit models because the shapes, sizes, and materials of the target objects are not known in advance. A convolution neural network (CNN) is another algorithm that can be used in conjunction with pressure sensor arrays for object detection. For e-nose arrays, PCA (i.e., a typical unsupervised ML algorithm) is widely used to implement feature clustering and classification.

The signal generated during the human perception process through various receptors is pre-processed in different transfer stages, and the process is completed in the brain. The unique sensory abilities of individual receptors, their selective responses, and signal processing at multiple levels ease the workload of the brain. Furthermore, the transmission of information through diverse channels at varying speeds facilitates the simultaneous processing of diverse types of data[176]. Similarly, in the bioinspired systems, we need to use materials with distinct mechanical characteristics, sensitivity, and selectivity to different stimuli. This fact has inspired several researchers to develop multimodal soft sensor arrays. However, mechanical isolation of various types of sensors should be attempted to minimise crosstalk and interference, as well as to improve their selectivity. Moreover, considering the different response times of different sensors could help trigger them one by one for processing to limit inter-sensor interference. Finding a trade-off between spatial resolution and interference for sensor arrays is an extremely difficult endeavour. The spatial resolution varies at the locations of different organs in the human body. Moreover, the spatial resolution can vary depending on the type of receptor. If the developed bioinspired systems can follow these categorisations, we

may be able to find an optimum trade-off between spatial resolution and interference. The data collected from multimodal sensors through a signal acquisition system could be processed using mathematical algorithms or, more often, ML algorithms to obtain better predictions[177-180]. However, multimodal signals from multimodal sensors are often redundant and complementary. Therefore, human experts should extract key features from the original data and provide them as inputs to ML. To avoid this difficult and time-consuming manual extraction, multimodal fusion algorithms could be applied. The structure of these algorithms is hierarchical and consists of at least three main levels: (1) data-level fusion to combine data from multimodal sensors; (2) feature-level fusion to extract features from the pre-processed data of each sensory modality and combine them to create a unified feature set; and (3) decision-level fusion to obtain feature-based classifications and their fusion to generate the final decision[181]. The signals obtained using multimodal sensors need to be labelled so that they can be processed using supervised ML algorithms, which is a time-consuming process. Moving towards semi- and unsupervised ML algorithms might be beneficial from the perspective of reducing data labelling, but doing so reduces accuracy. The use of hybrid supervised and unsupervised methods could be a solution to leverage the strengths of each method, but this approach requires better data integration, model selection, and performance evaluation. Apart from these data processing challenges, data collection over the long term will lead to security and privacy concerns related to the processes of data collection, transmission, and storage[182]. The high-level architecture of Internet of Things (IoT) components in healthcare can be divided into three layers: (1) the perception layer (i.e., sensing devices); (2) the network layer that connects the perception layer devices through wired and wireless connections; and (3) the application layer (i.e., end-user and data storage)[183]. By performing a security risk management analysis of each layer individually, the process of implementing appropriate security measures can be simplified. Wireless wearable sensors have attracted great interest in healthcare. Usually, sensor data are wirelessly communicated to a smartphone and then sent to a centralised cloud-based repository, where the relevant medical team can work on them. Wearable sensors usually have low power consumption because their power resources are limited. Therefore, the type of wireless technology used in each sensor is determined by bandwidth, power, and transmission range limitations. The data security of wireless sensors is extremely important, but the applied security measures should be consistent with the low-power requirements of the sensors, which translates into less efficient security[184]. The incorporation of various energy harvesting techniques can help mitigate the power source limitations of sensors and, therefore, enhance their security efficiency. The development of self-powered sensors, integration of energy harvesting sources with multifunctional sensors[185], and hybridisation of several energy harvesting mechanisms[186] could help elongate the lifetimes of sensor arrays, apart from the efforts to reduce sensor power consumption[187,188].

The development of new approaches that consider the personal needs of each patient opens new horizons in the diagnosis, treatment, and prevention of diseases. Despite all the mentioned challenges and considering the complex nature of diseases, multimodal sensor arrays that can simultaneously monitor multiple analytes or stimuli are the way forward for obtaining more information on the health status of patients and providing accurate diagnoses.

DECLARATIONS

Author contributions

Initiated the review and wrote the manuscript: Arab Hassani F

Availability of data and materials

Not applicable.

Financial support and sponsorship

Not applicable.

Conflicts of interest

The author declared that there are no conflicts of interest.

Ethical approval and consent to participate

Not applicable.

Consent for publication

Not applicable.

Copyright

REFERENCES

1. Alberts B, Heald R, Johnson A, et al. Molecular biology of the cell. 7th ed. New York, NY: Worldwide. Norton & Company; 2022. Available from: https://wwnorton.com/books/9780393884821. [Last accessed on 14 Aug 2023].
2. Lenau T, Stroble J, Stone R, Watkins S. An overview of biomimetic sensor technology. *Sensor Rev* 2009;29:112-9. DOI
3. Kandel ER, Koester JD, Mack SH, Siegelbaum SA. Principles of neural science. 6th ed. New York, NY: McGraw Hill; 2021. Available from: https://www.mheducation.co.uk/principles-of-neural-science-sixth-edition-9781259642234-emea. [Last accessed on 14 Aug 2023].
4. French AS, Torkkeli PH. Sensory receptors and mechanotransduction. In: Sperelakis N, editor. Cell Physiology Source Book. Elsevier; 2012. p. 633-47. Available from: https://edisciplinas.usp.br/pluginfile.php/5123031/mod_resource/content/2/Nicholas%20Sperelakis-Cell%20Physiology%20Source%20Book%2C%20Fourth%20Edition_%20Essentials%20of%20Membrane%20Biophysics-Academic%20Press%20%282012%29.pdf. [Last accessed on 14 Aug 2023].
5. Willis WD, Coggeshall RE. Sensory receptors and peripheral nerves. In: Sensory Mechanisms of the Spinal Cord. Boston: Springer US; 2004. p. 19-90. DOI
6. Abraira VE, Ginty DD. The sensory neurons of touch. *Neuron* 2013;79:618-39. DOI PubMed PMC
7. Chapleau MW, Sabharwal R. Methods of assessing vagus nerve activity and reflexes. *Heart Fail Rev* 2011;16:109-27. DOI PubMed PMC
8. Proske U, Gandevia SC. The proprioceptive senses: their roles in signaling body shape, body position and movement, and muscle force. *Physiol Rev* 2012;92:1651-97. DOI PubMed
9. Kobayashi S. Temperature receptors in cutaneous nerve endings are thermostat molecules that induce thermoregulatory behaviors against thermal load. *Temperature* 2015;2:346-51. DOI PubMed PMC
10. Wong KY. A retinal ganglion cell that can signal irradiance continuously for 10 hours. *J Neurosci* 2012;32:11478-85. DOI PubMed PMC
11. Tricas TC, Carlson BA. Electroreceptors and magnetoreceptors. In: Cell Physiology Source Book. Elsevier; 2012. p. 705-25. DOI
12. Winklhofer M, Kirschvink JL. A quantitative assessment of torque-transducer models for magnetoreception. *J R Soc Interface* 2010;7 Suppl 2:S273-89. DOI PubMed PMC
13. Wang J, Wang C, Cai P, et al. Artificial sense technology: emulating and extending biological senses. *ACS Nano* 2021;15:18671-8. DOI
14. Lee Y, Park J, Choe A, Cho S, Kim J, Ko H. Mimicking human and biological skins for multifunctional skin electronics. *Adv Funct Mater* 2020;30:1904523. DOI
15. Someya T, Bao Z, Malliaras GG. The rise of plastic bioelectronics. *Nature* 2016;540:379-85. DOI PubMed
16. Hong SY, Lee YH, Park H, et al. Stretchable active matrix temperature sensor array of polyaniline nanofibers for electronic skin. *Adv Mater* 2016;28:930-5. DOI
17. Zhang C, Ye WB, Zhou K, et al. Bioinspired artificial sensory nerve based on nafion memristor. *Adv Funct Mater* 2019;29:1808783. DOI
18. Murray AR, Fliesler SJ, Al-Ubaidi MR. Rhodopsin: the functional significance of asn-linked glycosylation and other post-translational modifications. *Ophthalmic Genet* 2009;30:109-20. DOI PubMed PMC
19. Kibenge FS, Strange RJ. Introduction to the anatomy and physiology of the major aquatic animal species in aquaculture. In: Aquaculture Pharmacology. Elsevier; 2021. p. 1-111. DOI
20. Zimmerman A, Bai L, Ginty DD. The gentle touch receptors of mammalian skin. *Science* 2014;346:950-4. DOI PubMed PMC
21. Chandrashekar J, Hoon MA, Ryba NJ, Zuker CS. The receptors and cells for mammalian taste. *Nature* 2006;444:288-94. DOI PubMed
22. Reisert J, Reingruber J. Ca^{2+}-activated Cl^- current ensures robust and reliable signal amplification in vertebrate olfactory receptor neurons. *Proc Natl Acad Sci U S A* 2019;116:1053-8. DOI PubMed PMC
23. Mittal R, Nguyen D, Patel AP, et al. Recent advancements in the regeneration of auditory hair cells and hearing restoration. *Front*

Mol Neurosci 2017;10:236. DOI PubMed PMC
24. Molday RS, Moritz OL. Photoreceptors at a glance. *J Cell Sci* 2015;128:4039-45. DOI PubMed PMC
25. Bertalmío M. The biological basis of vision: the retina. In: Vision Models for High Dynamic Range and Wide Colour Gamut Imaging. Elsevier; 2020. p. 11-46. DOI
26. Organisciak DT, Vaughan DK. Retinal light damage: mechanisms and protection. *Prog Retin Eye Res* 2010;29:113-34. DOI PubMed PMC
27. Gu L, Poddar S, Lin Y, et al. A biomimetic eye with a hemispherical perovskite nanowire array retina. *Nature* 2020;581:278-82. DOI
28. Stoddard P. Electrical signals. In: Breed MD, Moore J, editors. Encyclopedia of Animal Behavior. Elsevier; 2010. Available from: https://www.sciencedirect.com/referencework/9780080453378/encyclopedia-of-animal-behavior. [Last accessed on 14 Aug 2023].
29. England SJ, Robert D. The ecology of electricity and electroreception. *Biol Rev Camb Philos Soc* 2022;97:383-413. DOI PubMed
30. Newton KC, Gill AB, Kajiura SM. Electroreception in marine fishes: chondrichthyans. *J Fish Biol* 2019;95:135-54. DOI PubMed
31. Baker CVH, Modrell MS. Insights into electroreceptor development and evolution from molecular comparisons with hair cells. *Integr Comp Biol* 2018;58:329-40. DOI PubMed PMC
32. Shen Z, Zhu X, Majidi C, Gu G. Cutaneous ionogel mechanoreceptors for soft machines, physiological sensing, and amputee prostheses. *Adv Mater* 2021;33:e2102069. DOI PubMed
33. Aidley DJ. Mechanoreceptors. In: The Physiology of Excitable Cells. 4th ed. Cambridge: Cambridge University Press; 1998. p. 240-63. DOI
34. Iheanacho F, Vellipuram AR. Physiology, mechanoreceptors. Available from: https://www.ncbi.nlm.nih.gov/books/NBK541068/. [Last accessed on 14 Aug 2023].
35. Deflorio D, Di Luca M, Wing AM. Skin and mechanoreceptor contribution to tactile input for perception: a review of simulation models. *Front Hum Neurosci* 2022;16:862344. DOI PubMed PMC
36. Boughter JD, Munger SD. Taste receptors. In: Lennarz WJ, Lane MD, editors. Encyclopedia of Biological Chemistry. Waltham: Academic Press; 2013. p. 366-8. Available from: https://books.google.com/books?hl=zh-CN&lr=&id=ykUu06JQrjcC&oi=fnd&pg=PP2&dq=Boughter+J,+Munger+S.+Taste+Receptors.+Encyclopedia+of+Biological+Chemistry.&ots=eHzTqQTnW4&sig=z09pfOC_nBMkfR_PDSJOpBbbRCM#v=onepage&q&f=false. [Last accessed on 14 Aug 2023].
37. Shahbandi A, Choo E, Dando R. Receptor regulation in taste: can diet influence how we perceive foods? *J* 2018;1:106-15. DOI
38. Risso D, Drayna D, Morini G. Alteration, reduction and taste loss: main causes and potential implications on dietary habits. *Nutrients* 2020;12:3284. DOI PubMed PMC
39. Halpern BP. Constraints imposed on taste physiology by human taste reaction time data. *Neurosci Biobehav Rev* 1986;10:135-51. DOI PubMed
40. Williams J, Ringsdorf A. Human odour thresholds are tuned to atmospheric chemical lifetimes. *Philos Trans R Soc Lond B Biol Sci* 2020;375:20190274. DOI PubMed PMC
41. Bhatia-Dey N, Heinbockel T. The olfactory system as marker of neurodegeneration in aging, neurological and neuropsychiatric disorders. *Int J Environ Res Public Health* 2021;18:6976. DOI PubMed PMC
42. Stuck BA, Fadel V, Hummel T, Sommer JU. Subjective olfactory desensitization and recovery in humans. *Chem Senses* 2014;39:151-7. DOI PubMed
43. Pickles JO. Auditory pathways: anatomy and physiology. *Handb Clin Neurol* 2015;129:3-25. DOI
44. Kurabi A, Keithley EM, Housley GD, Ryan AF, Wong AC. Cellular mechanisms of noise-induced hearing loss. *Hear Res* 2017;349:129-37. DOI PubMed PMC
45. Leventhall G. What is infrasound? *Prog Biophys Mol Biol* 2007;93:130-7. DOI PubMed
46. Legatt AD. Electrophysiologic auditory tests. *Handb Clin Neurol* 2015;129:289-311. DOI
47. Soci C, Zhang A, Bao XY, Kim H, Lo Y, Wang D. Nanowire photodetectors. *J Nanosci Nanotechnol* 2010;10:1430-49. DOI
48. Lapierre RR, Robson M, Azizur-rahman KM, Kuyanov P. A review of III-V nanowire infrared photodetectors and sensors. *J Phys D: Appl Phys* 2017;50:123001. DOI
49. Tang J, Qin N, Chong Y, et al. Nanowire arrays restore vision in blind mice. *Nat Commun* 2018;9:786. DOI PubMed PMC
50. Seo J, Zhang K, Kim M, et al. Flexible phototransistors based on single-crystalline silicon nanomembranes. *Adv Opt Mater* 2016;4:120-5. DOI
51. Zheng X, Chen Z, Tao X, et al. Retina-inspired flexible photosensitive arrays based on selective photothermal conversion. *J Mater Chem C* 2022;11:252-9. DOI
52. Li Z, Cui Y, Zhong J. Recent advances in nanogenerators-based flexible electronics for electromechanical biomonitoring. *Biosens Bioelectron* 2021;186:113290. DOI
53. Guo ZH, Wang HL, Shao J, et al. Bioinspired soft electroreceptors for artificial precontact somatosensation. *Sci Adv* 2022;8:eabo5201. DOI PubMed PMC
54. Ma C, Xu D, Huang YC, et al. Robust flexible pressure sensors made from conductive micropyramids for manipulation tasks. *ACS Nano* 2020;14:12866-76. DOI
55. Shang C, Xu Q, Liang N, Zhang J, Li L, Peng Z. Multi-parameter e-skin based on biomimetic mechanoreceptors and stress field sensing. *npj Flex Electron* 2023;7:19. DOI
56. Nguyen TD, Lee JS. Recent development of flexible tactile sensors and their applications. *Sensors* 2021;22:50. DOI PubMed PMC
57. Zhang J, Yao H, Mo J, et al. Finger-inspired rigid-soft hybrid tactile sensor with superior sensitivity at high frequency. *Nat Commun*

2022;13:5076. DOI PubMed PMC
58. Yang Y, Zhang H, Chen J, et al. Single-electrode-based sliding triboelectric nanogenerator for self-powered displacement vector sensor system. *ACS Nano* 2013;7:7342-51. DOI
59. Arab Hassani F, Mogan RP, Gammad GGL, et al. Toward self-control systems for neurogenic underactive bladder: a triboelectric nanogenerator sensor integrated with a bistable micro-actuator. *ACS Nano* 2018;12:3487-501. DOI
60. Hassani FA, Lee C. A triboelectric energy harvester using low-cost, flexible, and biocompatible ethylene vinyl acetate (EVA). *J Microelectromech Syst* 2015;24:1338-45. DOI
61. Kim C, Lee KK, Kang MS, et al. Artificial olfactory sensor technology that mimics the olfactory mechanism: a comprehensive review. *Biomater Res* 2022;26:40. DOI PubMed PMC
62. Chouhdry HH, Lee DH, Bag A, Lee NE. A flexible artificial chemosensory neuronal synapse based on chemoreceptive ionogel-gated electrochemical transistor. *Nat Commun* 2023;14:821. DOI PubMed PMC
63. Moon D, Cha YK, Kim SO, Cho S, Ko HJ, Park TH. FET-based nanobiosensors for the detection of smell and taste. *Sci China Life Sci* 2020;63:1159-67. DOI PubMed
64. Zhao T, Wang Q, Du A. Self-powered flexible sour sensor for detecting ascorbic acid concentration based on triboelectrification/enzymatic-reaction coupling effect. *Sensors* 2021;21:373. DOI PubMed PMC
65. Prasad BB, Tiwari MP. Molecularly imprinted nanomaterial-based highly sensitive and selective medical devices. In: Tiwari A, Ramalingam M, Kobayashi H, Turner APF, editors. Biomedical materials and diagnostic devices. Scrivener Publishing LLC; 2012. p. 339-91. DOI
66. Wang J, Sakai K, Kiwa T. All-in-one terahertz taste sensor: integrated electronic and bioelectronic tongues. *Sens Diagn* 2023;2:620-6. DOI
67. Nag A, Mukhopadhyay SC. Fabrication and implementation of printed sensors for taste sensing applications. *Sens Actuator A Phys* 2018;269:53-61. DOI
68. Jung YH, Hong SK, Wang HS, et al. Speech recognition: flexible piezoelectric acoustic sensors and machine learning for speech processing. *Adv Mater* 2020;32:2070259. DOI
69. Viola G, Chang J, Maltby T, et al. Bioinspired multiresonant acoustic devices based on electrospun piezoelectric polymeric nanofibers. *ACS Appl Mater Interfaces* 2020;12:34643-57. DOI PubMed PMC
70. Wang HS, Hong SK, Han JH, et al. Biomimetic and flexible piezoelectric mobile acoustic sensors with multiresonant ultrathin structures for machine learning biometrics. *Sci Adv* 2021;7:eabe5683. DOI PubMed PMC
71. Svechtarova MI, Buzzacchera I, Toebes BJ, Lauko J, Anton N, Wilson CJ. Sensor devices inspired by the five senses: a review. *Electroanalysis* 2016;28:1201-41. DOI
72. Johnson KJ, Rose-Pehrsson SL. Sensor array design for complex sensing tasks. *Annu Rev Anal Chem* 2015;8:287-310. DOI PubMed
73. Kashyap V, Yin J, Xiao X, Chen J. Bioinspired nanomaterials for wearable sensing and human-machine interfacing. *Nano Res* 2023;1-17. DOI
74. Parameswaran C, Gupta D. Large area flexible pressure/strain sensors and arrays using nanomaterials and printing techniques. *Nano Converg* 2019;6:28. DOI PubMed PMC
75. Yeo JC, Lim CT. Emerging flexible and wearable physical sensing platforms for healthcare and biomedical applications. *Microsyst Nanoeng* 2016;2:16043. DOI PubMed PMC
76. Lu K, Li L, Jiang S, et al. Advanced bioinspired organic sensors for future-oriented intelligent applications. *Adv Sens Res* 2023;2:2200066. DOI
77. Liu Z, Kong J, Qu M, Zhao G, Zhang C. Progress in data acquisition of wearable sensors. *Biosensors* 2022;12:889. DOI PubMed PMC
78. Marquez AV, McEvoy N, Pakdel A. Organic electrochemical transistors (OECTs) toward flexible and wearable bioelectronics. *Molecules* 2020;25:5288. DOI PubMed PMC
79. Braendlein M, Lonjaret T, Leleux P, Badier JM, Malliaras GG. Voltage amplifier based on organic electrochemical transistor. *Adv Sci* 2017;4:1600247. DOI PubMed PMC
80. Li Z, Wei Q, Han J. Editorial: array-based sensing techniques for clinical, agricultural biotechnology, and environmental analysis. *Front Chem* 2021;9:654707. DOI PubMed PMC
81. Duan Y, He S, Wu J, Su B, Wang Y. Recent progress in flexible pressure sensor arrays. *Nanomaterials* 2022;12:2495. DOI PubMed PMC
82. Dincer C, Bruch R, Costa-Rama E, et al. Disposable sensors in diagnostics, food, and environmental monitoring. *Adv Mater* 2019;31:e1806739. DOI
83. Yang Y, Gao W. Wearable and flexible electronics for continuous molecular monitoring. *Chem Soc Rev* 2019;48:1465-91. DOI
84. Cheng S, Gu Z, Zhou L, et al. Recent progress in intelligent wearable sensors for health monitoring and wound healing based on biofluids. *Front Bioeng Biotechnol* 2021;9:765987. DOI PubMed PMC
85. Dong W, Wang Y, Zhou Y, et al. Soft human-machine interfaces: design, sensing and stimulation. *Int J Intell Robot Appl* 2018;2:313-38. DOI
86. Kim DH, Lu N, Ma R, et al. Epidermal electronics. *Science* 2011;333:838-43. DOI
87. Arab Hassani F, Jin H, Yokota T, Someya T, Thakor NV. Soft sensors for a sensing-actuation system with high bladder voiding efficiency. *Sci Adv* 2020;6:eaba0412. DOI PubMed PMC

88. Ren L, Li B, Wei G, et al. Biology and bioinspiration of soft robotics: actuation, sensing, and system integration. *iScience* 2021;24:103075. DOI PubMed PMC
89. Bhave G, Chen JC, Singer A, Sharma A, Robinson JT. Distributed sensor and actuator networks for closed-loop bioelectronic medicine. *Mater Today* 2021;46:125-35. DOI PubMed PMC
90. Yoo S, Yang T, Park M, et al. Responsive materials and mechanisms as thermal safety systems for skin-interfaced electronic devices. *Nat Commun* 2023;14:1024. DOI PubMed PMC
91. Röder PV, Wu B, Liu Y, Han W. Pancreatic regulation of glucose homeostasis. *Exp Mol Med* 2016;48:e219. DOI PubMed PMC
92. Grose DN, O'brien CL, Castle DJ. Type 1 diabetes and an insulin pump: an iterative review of qualitative literature. *Pract Diab* 2017;34:281-7c. DOI
93. Ilami M, Bagheri H, Ahmed R, Skowronek EO, Marvi H. Materials, actuators, and sensors for soft bioinspired robots. *Adv Mater* 2021;33:e2003139. DOI PubMed
94. Li S, Wang KW. Plant-inspired adaptive structures and materials for morphing and actuation: a review. *Bioinspir Biomim* 2016;12:011001. DOI
95. Speck T, Cheng T, Klimm F, et al. Plants as inspiration for material-based sensing and actuation in soft robots and machines. *MRS Bulletin* 2023. DOI
96. Yang M, Wu J, Jiang W, Hu X, Iqbal MI, Sun F. Bioinspired and hierarchically textile□structured soft actuators for healthcare wearables. *Adv Funct Mater* 2023;33:2210351. DOI
97. Lan R, Shen W, Yao W, Chen J, Chen X, Yang H. Bioinspired humidity-responsive liquid crystalline materials: from adaptive soft actuators to visualized sensors and detectors. *Mater Horiz* 2023;10:2824-44. DOI
98. Jiang L, Lu G, Zeng Y, et al. Flexible ultrasound-induced retinal stimulating piezo-arrays for biomimetic visual prostheses. *Nat Commun* 2022;13:3853. DOI PubMed PMC
99. Lee HJ, Baik S, Hwang GW, et al. An electronically perceptive bioinspired soft wet-adhesion actuator with carbon nanotube-based strain sensors. *ACS Nano* 2021;15:14137-48. DOI
100. Ren J, Liu Q, Pei Y, et al. Bioinspired energy storage and harvesting devices. *Adv Mater Technol* 2021;6:2001301. DOI
101. Peng L, Zhang Y, Wang J, et al. Slug-inspired magnetic soft millirobot fully integrated with triboelectric nanogenerator for on-board sensing and self-powered charging. *Nano Energy* 2022;99:107367. DOI
102. Arab Hassani F, Shi Q, Wen F, et al. Smart materials for smart healthcare- moving from sensors and actuators to self-sustained nanoenergy nanosystems. *Smart Mater Med* 2020;1:92-124. DOI
103. Wang Y, Hong M, Venezuela J, Liu T, Dargusch M. Expedient secondary functions of flexible piezoelectrics for biomedical energy harvesting. *Bioact Mater* 2023;22:291-311. DOI PubMed PMC
104. Wang X, Yin Y, Yi F, et al. Bioinspired stretchable triboelectric nanogenerator as energy-harvesting skin for self-powered electronics. *Nano Energy* 2017;39:429-36. DOI
105. Tauber FJ, Slesarenko V. Early career scientists converse on the future of soft robotics. *Front Robot AI* 2023;10:1129827. DOI PubMed PMC
106. Zhi C, Shi S, Zhang S, et al. Bioinspired all-fibrous directional moisture-wicking electronic skins for biomechanical energy harvesting and all-range health sensing. *Nanomicro Lett* 2023;15:60. DOI PubMed PMC
107. Li W, Pei Y, Zhang C, Kottapalli AGP. Bioinspired designs and biomimetic applications of triboelectric nanogenerators. *Nano Energy* 2021;84:105865. DOI
108. Shin D, Han HJ, Kim W, et al. Bioinspired piezoelectric nanogenerators based on vertically aligned phage nanopillars. *Energy Environ Sci* 2015;8:3198-203. DOI
109. Senthil R, Yuvaraj S. A comprehensive review on bioinspired solar photovoltaic cells. *Int J Energy Res* 2019;43:1068-81. DOI
110. Liu R, Wang ZL, Fukuda K, Someya T. Flexible self-charging power sources. *Nat Rev Mater* 2022;7:870-86. DOI
111. Valle M. Bioinspired sensor systems. *Sensors* 2011;11:10180-6. DOI PubMed PMC
112. Jung YH, Park B, Kim JU, Kim TI. Bioinspired electronics for artificial sensory systems. *Adv Mater* 2019;31:e1803637. DOI PubMed
113. Xiao K, Wan C, Jiang L, Chen X, Antonietti M. Bioinspired ionic sensory systems: the successor of electronics. *Adv Mater* 2020;32:e2000218. DOI
114. Li P, Anwar Ali HP, Cheng W, Yang J, Tee BCK. Bioinspired prosthetic interfaces. *Adv Mater Technol* 2020;5:1900856. DOI
115. Xue J, Zou Y, Deng Y, Li Z. Bioinspired sensor system for health care and human-machine interaction. *EcoMat* 2022;4:e12209. DOI
116. Choi C, Choi MK, Liu S, et al. Human eye-inspired soft optoelectronic device using high-density MoS_2-graphene curved image sensor array. *Nat Commun* 2017;8:1664. DOI PubMed PMC
117. Song WJ, Lee Y, Jung Y, et al. Soft artificial electroreceptors for noncontact spatial perception. *Sci Adv* 2021;7:eabg9203. DOI PubMed PMC
118. Yu X, Xie Z, Yu Y, et al. Skin-integrated wireless haptic interfaces for virtual and augmented reality. *Nature* 2019;575:473-9. DOI
119. Zhou Q, Ji B, Wei Y, et al. A bio-inspired cilia array as the dielectric layer for flexible capacitive pressure sensors with high sensitivity and a broad detection range. *J Mater Chem A* 2019;7:27334-46. DOI
120. Kim SH, Baek GW, Yoon J, et al. A bioinspired stretchable sensory-neuromorphic system. *Adv Mater* 2021;33:e2104690. DOI PubMed

121. Wang J, Zhu Y, Wu Z, et al. Wearable multichannel pulse condition monitoring system based on flexible pressure sensor arrays. *Microsyst Nanoeng* 2022;8:16. DOI PubMed PMC
122. Fan W, He Q, Meng K, et al. Machine-knitted washable sensor array textile for precise epidermal physiological signal monitoring. *Sci Adv* 2020;6:eaay2840. DOI PubMed PMC
123. Huang S, Zhang T, Li H, et al. Flexible tongue electrode array system for in vivo mapping of electrical signals of taste sensation. *ACS Sens* 2021;6:4108-17. DOI
124. Yeom J, Choe A, Lim S, Lee Y, Na S, Ko H. Soft and ion-conducting hydrogel artificial tongue for astringency perception. *Sci Adv* 2020;6:eaba5785. DOI PubMed PMC
125. Lorwongtragool P, Baumann RR, Sowade E, Watthanawisuth N, Kerdcharoen T. A Zigbee-based wireless wearable electronic nose using flexible printed sensor array. In: 2013 IEEE 5th International Nanoelectronics Conference; 2013 Jan 2-4; Singapore. IEEE; 2013. p. 291-3. DOI
126. Zheng Y, Li H, Shen W, Jian J. Wearable electronic nose for human skin odor identification: a preliminary study. *Sens Actuator A Phys* 2019;285:395-405. DOI
127. Yang C, Xiang Y, Liao B, Hu X. 3D-printed bionic ear for sound identification and localization based on in situ polling of PVDF-TrFE film. *Macromol Biosci* 2023;23:2200374. DOI
128. Shin YE, Park YJ, Ghosh SK, Lee Y, Park J, Ko H. Ultrasensitive multimodal tactile sensors with skin-inspired microstructures through localized ferroelectric polarization. *Adv Sci* 2022;9:2105423. DOI
129. Hua Q, Sun J, Liu H, et al. Skin-inspired highly stretchable and conformable matrix networks for multifunctional sensing. *Nat Commun* 2018;9:244. DOI PubMed PMC
130. Curcio CA, Sloan KR, Kalina RE, Hendrickson AE. Human photoreceptor topography. *J Comp Neurol* 1990;292:497-523. DOI PubMed
131. Kalmijn AJ. The electric sense of sharks and rays. *J Exp Biol* 1971;55:371-83. DOI
132. Collin SP. Electroreception in vertebrates and invertebrates. In: Breed MD, Moore J, editors. Encyclopedia of Animal Behavior. Elsevier; 2010. p. 611-20. Available from: https://www.sciencedirect.com/referencework/9780080453378/encyclopedia-of-animal-behavior. [Last accessed on 14 Aug 2023].
133. Gonzalez-Franco M, Lanier J. Model of illusions and virtual reality. *Front Psychol* 2017;8:1125. DOI PubMed PMC
134. Syed TA, Siddiqui MS, Abdullah HB, et al. In-depth review of augmented reality: tracking technologies, development tools, ar displays, collaborative ar, and security concerns. *Sensors* 2022;23:146. DOI PubMed PMC
135. Stein BE, Stanford TR, Rowland BA. Multisensory integration and the society for neuroscience: then and now. *J Neurosci* 2020;40:3-11. DOI PubMed PMC
136. Liu Y, Yiu CK, Zhao Z, et al. Soft, miniaturized, wireless olfactory interface for virtual reality. *Nat Commun* 2023;14:2297. DOI PubMed PMC
137. Tauber F, Desmulliez M, Piccin O, Stokes AA. Perspective for soft robotics: the field's past and future. *Bioinspir Biomim* 2023;18:035001. DOI PubMed
138. Lopez-Ojeda W, Amarendra P, Mandy A, Oakley AM. Anatomy, skin (Integument). Available from: https://www.ncbi.nlm.nih.gov/books/NBK441980/. [Last accessed on 14 Aug 2023].
139. Caire MJ, Reddy V, Varacallo M. Physiology, synapse. Available from: https://www.ncbi.nlm.nih.gov/books/NBK526047/. [Last accessed on 14 Aug 2023].
140. Kebe M, Gadhafi R, Mohammad B, Sanduleanu M, Saleh H, Al-Qutayri M. Human vital signs detection methods and potential using radars: a review. *Sensors* 2020;20:1454. DOI PubMed PMC
141. Ahmad R, Dalziel JE. G protein-coupled receptors in taste physiology and pharmacology. *Front Pharmacol* 2020;11:587664. DOI PubMed PMC
142. Essick GK, Trulsson M. Tactile sensation in oral region. In: Binder MD, Hirokawa N, Windhorst U, editors. Encyclopedia of Neuroscience. Berlin: Springer Berlin Heidelberg; 2009. p. 3999-4005. DOI
143. Kaczmarek KA. The tongue display unit (TDU) for electrotactile spatiotemporal pattern presentation. *Sci Iran D Comput Sci Eng Electr Eng* 2011;18:1476-85. DOI PubMed PMC
144. Krautwurst D. Human olfactory receptor families and their odorants. *Chem Biodivers* 2008;5:842-52. DOI PubMed
145. Ramgir NS. Electronic nose based on nanomaterials: issues, challenges, and prospects. *ISRN Nanomaterials* 2013;2013:1-21. DOI
146. Manley GA, Lukashkin AN, Simões P, Burwood GWS, Russell IJ. The mammalian ear: physics and the principles of evolution. *Acoust Today* 2018;14:1-9. Available from: https://acousticstoday.org/wp-content/uploads/2019/03/The-Mammalian-Ear-Physics-and-the-Principles-of-Evolution.pdf. [Last accessed on 14 Aug 2023].
147. Sheikh A, Bint-e-zainab, Shabbir K, Imtiaz A. Structure and physiology of human ear involved in hearing. In: Naz S, editor. Auditory System - Function and Disorders. IntechOpen; 2022. DOI
148. Xiang L, Wang Y, Xia F, et al. An epidermal electronic system for physiological information acquisition, processing, and storage with an integrated flash memory array. *Sci Adv* 2022;8:eabp8075. DOI PubMed PMC
149. Liu M, Zhang Y, Wang J, et al. A star-nose-like tactile-olfactory bionic sensing array for robust object recognition in non-visual environments. *Nat Commun* 2022;13:79. DOI PubMed PMC
150. Gao Y, Nguyen DT, Yeo T, et al. A flexible multiplexed immunosensor for point-of-care in situ wound monitoring. *Sci Adv* 2021;7:eabg9614. DOI PubMed PMC
151. Kim J, Kim M, Lee MS, et al. Wearable smart sensor systems integrated on soft contact lenses for wireless ocular diagnostics. *Nat*

Commun 2017;8:14997. DOI PubMed PMC
152. Guo S, Wu K, Li C, et al. Integrated contact lens sensor system based on multifunctional ultrathin MoS_2 transistors. *Matter* 2021;4:969-85. DOI PubMed PMC
153. Gao W, Emaminejad S, Nyein HYY, et al. Fully integrated wearable sensor arrays for multiplexed in situ perspiration analysis. *Nature* 2016;529:509-14. DOI PubMed PMC
154. Beduk T, Beduk D, Hasan MR, et al. Smartphone-based multiplexed biosensing tools for health monitoring. *Biosensors* 2022;12:583. DOI PubMed PMC
155. Lee S, Kim SR, Jeon KH, et al. A fabric-based wearable sensor for continuous monitoring of decubitus ulcer of subjects lying on a bed. *Sci Rep* 2023;13:5773. DOI PubMed PMC
156. Wu X, Li E, Liu Y, et al. Artificial multisensory integration nervous system with haptic and iconic perception behaviors. *Nano Energy* 2021;85:106000. DOI
157. Yu J, Zhang K, Deng Y. Recent progress in pressure and temperature tactile sensors: Principle, classification, integration and outlook. *Soft Sci* 2021;1:6. DOI
158. Duan S, Shi Q, Wu J. Multimodal sensors and ml-based data fusion for advanced robots. *Adv Intell Syst* 2022;4:2200213. DOI
159. Matsuda R, Mizuguchi S, Nakamura F, et al. Highly stretchable sensing array for independent detection of pressure and strain exploiting structural and resistive control. *Sci Rep* 2020;10:12666. DOI PubMed PMC
160. Cho S, Han H, Park H, et al. Wireless, multimodal sensors for continuous measurement of pressure, temperature, and hydration of patients in wheelchair. *npj Flex Electron* 2023;7:8. DOI
161. Hozumi S, Honda S, Arie T, Akita S, Takei K. Multimodal wearable sensor sheet for health-related chemical and physical monitoring. *ACS Sens* 2021;6:1918-24. DOI PubMed
162. Philip J. Photopyroelectric spectroscopy: a direct photothermal technique to evaluate thermal properties of condensed matter. In: Thakur SN, Rai VN, Singh JP, editors. Photoacoustic and Photothermal Spectroscopy. Elsevier; 2023. p. 231-43. DOI
163. Sin ML, Mach KE, Wong PK, Liao JC. Advances and challenges in biosensor-based diagnosis of infectious diseases. *Expert Rev Mol Diagn* 2014;14:225-44. DOI PubMed PMC
164. Pauliukaite R, Voitechovič E. Multisensor systems and arrays for medical applications employing naturally-occurring compounds and materials. *Sensors* 2020;20:3551. DOI PubMed PMC
165. Lee S, Franklin S, Hassani FA, et al. Nanomesh pressure sensor for monitoring finger manipulation without sensory interference. *Science* 2020;370:966-70. DOI
166. Mannsfeld SC, Tee BC, Stoltenberg RM, et al. Highly sensitive flexible pressure sensors with microstructured rubber dielectric layers. *Nat Mater* 2010;9:859-64. DOI
167. Lim HR, Kim HS, Qazi R, Kwon YT, Jeong JW, Yeo WH. Advanced soft materials, sensor integrations, and applications of wearable flexible hybrid electronics in healthcare, energy, and environment. *Adv Mater* 2020;32:e1901924. DOI
168. Rogers JA, Someya T, Huang Y. Materials and mechanics for stretchable electronics. *Science* 2010;327:1603-7. DOI PubMed
169. Wang C, Hwang D, Yu Z, et al. User-interactive electronic skin for instantaneous pressure visualization. *Nat Mater* 2013;12:899-904. DOI
170. Li Y, Long J, Chen Y, Huang Y, Zhao N. Crosstalk-free, high-resolution pressure sensor arrays enabled by high-throughput laser manufacturing. *Adv Mater* 2022;34:e2200517. DOI PubMed
171. Wang R, Hu S, Zhu W, et al. Recent progress in high-resolution tactile sensor array: from sensor fabrication to advanced applications. *Prog Nat Sci Mater Inter* 2023;33:55-66. DOI
172. Nan X, Xu Z, Cao X, et al. A review of epidermal flexible pressure sensing arrays. *Biosensors* 2023;13:656. DOI PubMed PMC
173. Yao G, Yin C, Wang Q, et al. Flexible bioelectronics for physiological signals sensing and disease treatment. *J Materiomics* 2020;6:397-413. DOI
174. Ates HC, Nguyen PQ, Gonzalez-Macia L, et al. End-to-end design of wearable sensors. *Nat Rev Mater* 2022;7:887-907. DOI PubMed PMC
175. Zhang S, Suresh L, Yang J, Zhang X, Tan SC. Augmenting sensor performance with machine learning towards smart wearable sensing electronic systems. *Adv Intell Syst* 2022;4:2100194. DOI
176. Zeng X, Hu Y. Sensation and perception of a bioinspired flexible smart sensor system. *ACS Nano* 2021;15:9238-43. DOI PubMed
177. Faura G, Boix-Lemonche G, Holmeide AK, et al. Colorimetric and electrochemical screening for early detection of diabetes mellitus and diabetic retinopathy-application of sensor arrays and machine learning. *Sensors* 2022;22:718. DOI PubMed PMC
178. Luo Y, Abidian MR, Ahn JH, et al. Technology roadmap for flexible sensors. *ACS Nano* 2023;17:5211-95. DOI
179. Zhang Y, Hu Y, Jiang N, Yetisen AK. Wearable artificial intelligence biosensor networks. *Biosens Bioelectron* 2022;219:114825. DOI
180. Tu J, Wang M, Li W, et al. Electronic skins with multimodal sensing and perception. *Soft Sci* 2023;3:25. DOI
181. Muhammad G, Alshehri F, Karray F, Saddik AE, Alsulaiman M, Falk TH. A comprehensive survey on multimodal medical signals fusion for smart healthcare systems. *Information Fusion* 2021;76:355-75. DOI
182. Christodouleas DC, Kaur B, Chorti P. From point-of-care testing to ehealth diagnostic devices (eDiagnostics). *ACS Cent Sci* 2018;4:1600-16. DOI PubMed PMC
183. Affia AO, Finch H, Jung W, Samori IA, Potter L, Palmer X. IoT health devices: exploring security risks in the connected landscape. *IoT* 2023;4:150-82. DOI

184. Bhatti DS, Saleem S, Imran A, et al. A survey on wireless wearable body area networks: a perspective of technology and economy. *Sensors* 2022;22:7722. DOI PubMed PMC
185. Liu D, Gao Y, Zhou L, Wang J, Wang ZL. Recent advances in high-performance triboelectric nanogenerators. *Nano Res* 2023. DOI
186. Liu H, Fu H, Sun L, Lee C, Yeatman EM. Hybrid energy harvesting technology: from materials, structural design, system integration to applications. *Renew Sust Energ* 2021;137:110473. DOI
187. Dagdeviren C, Yang BD, Su Y, et al. Conformal piezoelectric energy harvesting and storage from motions of the heart, lung, and diaphragm. *Proc Natl Acad Sci U S A* 2021;118:e2110994118. DOI PubMed PMC
188. Dai C, Chen H, Wang L, et al. A highly temperature- and pressure-sensitive soft sensor self-powered by a galvanic cell design. *J Mater Chem A* 2022;10:4408-17. DOI